galaxies

MDPI

Article

# Physics of "Cold" Disk Accretion onto Black Holes Driven by Magnetized Winds

**Sergey Bogovalov**

National Research Nuclear University (MEPHI), Kashirskoje Shosse, 31, 115409 Moscow, Russia; ss433@mail.ru; Tel.: +7-495-788-5699

Received: 30 October 2018; Accepted: 3 January 2019; Published: 14 January 2019

check for updates

**Abstract:** Disk accretion onto black holes is accompanied by collimated outflows (jets). In active galactic nuclei (AGN), the kinetic energy flux of the jet (jet power or kinetic luminosity) may exceed the bolometric luminosity of the disk by a few orders of magnitude. This may be explained in the framework of the so called "cold" disk accretion. In this regime of accretion, the disk is radiatively inefficient because practically all the energy released at the accretion is carried out by the magnetized wind. This wind also provides efficient loss of the angular momentum by the matter in the disk. In this review, the physics of the accretion driven by the wind is considered from first principles. It is shown that the magnetized wind can efficiently carry out angular momentum and energy of the matter of the disk. The conditions when this process dominates conventional loss of the angular momentum due to turbulent viscosity are discussed. The "cold" accretion occurs when the viscous stresses in the disk can be neglected in comparison with impact of the wind on the accretion. Two problems crucial for survival of the model of "cold" accretion are considered. The first one is existence of the magnetohydrodynamical solutions for disk accretion purely due to the angular momentum loss by the wind. Another problem is the ability of the model to reproduce observations which demonstrate existence of the sources with kinetic power of jets 2–3 orders of magnitude exceeding the bolometric luminosity of disks. The solutions of the problem in similar prescriptions and numerical solutions without such an assumption are discussed. Calculations of the "unavoidable" radiation from the "cold" disk and the ratio of the jet power of the SMBH to the bolometric luminosity of the accretion disk around a super massive black hole are given in the framework of the Shakura and Sunyaev paradigm of an optically thick $\alpha$-disk. The exploration of the Fundamental Plane of Black Holes allows us to obtain semi empirical equations that determine the bolometric luminosity and the ratio of the luminosities as functions of the black hole mass and accretion rate.

**Keywords:** MHD–accretion; accretion discs–jets; AGN

## 1. Introduction

Classical works on the physics of accretion [1–3] laid the foundations of the theory of disk accretion onto relativistic objects, neutron stars and black holes. In the model of Shakura and Sunyaev [3] (hereafter, SS model), every particle loses angular momentum due to viscous stresses arising in a turbulent plasma. In the geometrically thin and optically thick accretion disks, all the gravitational energy released at the accretion is carried out by radiation.

The bolometric luminosity of a disk accreting onto a nonrotating black hole can be represented as $L_{bol} = \eta \dot{M} c^2$, where $\dot{M}$ is the rate of accretion, $c$ is the speed of light and $\eta$ is the efficiency of transformation of the rest of the mass into the radiation during the accretion onto a Schwarzschild black hole $\eta \approx 0.1$. It is also convenient to work with the dimensionless mass of the black hole $m = M/M_{\odot}$, where $M_{\odot}$ is the solar mass, and dimensionless luminosity expressed in units of the Eddington luminosity $L_{Edd} = 4\pi G m_p M c/\sigma_T$, where $G$ is the gravitational constant, $m_p$ is the proton mass, and $\sigma_T$ is the Thomson cross-section. At Eddington luminosity, the force arising in Thomson scattering of photons of radiation on an electron equals the force of gravitational attraction of the proton compensating the electric charge of the electron. Correspondingly, the Eddington accretion rate is introduced as $\dot{M}_{Edd} = L_{Edd}/\eta c^2$. Dimensionless accretion rate $\dot{m} = \dot{M}/\dot{M}_{Edd}$. In the standard SS disk, accretion $L_{bol}/L_{Edd} = \dot{m}$.

Observations of AGNs revealed rather dramatic deviations of the theory from reality. The galactic center of our galaxy Sgr A* is especially interesting in this regard. Sgr A* is surprisingly faint despite the rich gas reservoir in its immediate surroundings that should provide a high accretion rate. The accretion onto the SMBH in the Galactic center should be $\dot{M} \sim 10^{-6}$ $M_\odot$/year [4] at Bondi radius. For the mass of SMBH, $M = 4 \times 10^6$ $\dot{M}_{Edd} = 0.072$ $M_\odot$/year giving the accretion rate $\dot{m} \sim 10^{-5}$. However, the bolometric luminosity is no more than $\sim 10^{36}$ ergs$^{-1}$. This corresponds to $L_{bol}/L_{Edd} = 2.5 \times 10^{-9}$, which is 3–4 orders of magnitude below the value that should be expected in the standard SS disk. This is not an isolated case.

The faintness of Sgr A* led to the development of theoretical models with radiatively inefficient accretion flows (RIAFs). One of the models is the advection dominated accretion flow (ADAF) [5], in which the low luminosity is explained by the combination of a high ratio of radial to tangential gas velocities, and the decoupling of hot protons and cold electrons in low density gas. However, this solution has numerous problems both in the assumptions used and in comparing with the observations. For example, the presence of the magnetic field in the accreted material violates one of the basic assumptions of ADIOS that radiation efficiency of the disk is low [6]. The detection of linear polarization and the low electron densities estimated from the Faraday rotation measure rules out the large accretion rate of the standard ADAF model. This led to the development of convection dominated accretion flow models (CDAFs) [7,8], which favor lower accretion rates and shallower density profiles. The last set of models are models with substantial mass loss like advection-dominated inflow–outflow solutions (ADIOS) [9–11] or jet models [12,13].

While astrophysicists tried to explain the low luminosity of disks, another spectacular property was discovered. Accretion at a low rate is accompanied by an impressive phenomena, which was not expected in the standard models. X-ray binaries and AGN produce jets, well collimated flows of plasma, propagating on a large distance from the source. It has been found that power of the jets from AGN is often much greater than the bolometric luminosity of the disk. For example, the famous galaxy M87 is a characteristic example of an AGN with a very large kinetic luminosity $\sim 10^{44}$ erg/s [14,15] in comparison with the bolometric luminosity of the disk not exceeding $10^{42}$ erg/s [16]. The example of M87 is also not an isolated case.

It is necessary to keep in mind that estimation of the kinetic and bolometric luminosities of the jets is not a simple task for observers. Starting with the paper [17], jet power in radio galaxies and quasars were estimated using energetics and lifetimes of extended double radio sources. The ratio of kinetic-to-bolometric luminosity can be estimated also from radio and X-ray data. The works [18–24] argued that the radio and X-ray luminosities are likely to be related to the kinetic and bolometric luminosities, respectively. Exploration of these methods shows that, in a large fraction of AGNs, the jet kinetic luminosity exceeds the bolometric luminosity [25–31].

Other estimates follows from gamma-ray astronomy. The jet power in 191 quasars detected by the Fermi Large Area Telescope (LAT) in gamma rays, systematically exceeds the bolometric luminosity [32].

Indirect evidence of high kinetic luminosity of an outflow exceeding the bolometric luminosity is provided by observations of the Galactic Center in TeV gamma-rays [33]. To explain the observed diffuse flux of the VHE gamma-rays from the Galactic Center region, the production rate of protons accelerated up to 1 PeV should be $\sim 10^{38}$ erg/s. Assuming that the accelerator of protons is powered by the kinetic energy of the outflow (a wind or jets) from the SMBH in the Galactic Center (Sgr A*), even in the case of 100% conversion of the bulk kinetic energy to non thermal particles, the kinetic luminosity of the outflow would be two orders of magnitude larger than the bolometric luminosity of Sgr A*, which is estimated to be close to $10^{36}$ erg/s [34].

Sometimes, the jet power exceeds the Eddington limit. Observations of the very powerful and bright in gamma-rays AGN 3C 454.3 during the outbursts of this object show that the apparent luminosity in GeV gamma-rays could exceed $10^{50}$ erg/s [35–38]. The mass of the black hole in this AGN is estimated in the region (0.5–4) $\times$ $10^9$ M$\odot$. Thus, the Eddington luminosity is in the range of (0.6–5) $\times$ $10^{47}$ erg/s. Because of the Doppler boosting effect, the intrinsic gamma-ray luminosity of this source is much smaller, by several orders of magnitude, than the apparent luminosity. However, the estimates of the jet kinetic luminosity in any realistic scenario give a value exceeding the Eddington luminosity [39]. In general, the estimates of the bolometric and kinetic luminosities are model dependent [40]. Nevertheless, it is unlikely that the estimated values differ from the actual values more than an order of magnitude. Therefore, it is difficult to avoid a conclusion that some AGNs demonstrate extremely high kinetic luminosities of jets which are not only above the bolometric luminosity, but in some cases can exceed the Eddington luminosity of the central SMBH.

Compilation of data about X-ray binaries and AGN results in the following general picture. At high accretion rates, the accretion occurs in accordance with the SS model. The disk is bright and there is no (or there is only weak) evidence of jets [41]. At accretion rate $\dot{m} < 10^{-2} - 10^{-1}$, the disk becomes radiatively inefficient and accretion is accompanied by powerful jets. This picture is a challenge for astrophysicists. It is necessary to answer two key questions. The first one is why the accretion process is radiatively inefficient at low accretion rates and why jets with the kinetic luminosity exceeding the bolometric luminosity are produced in this regime of accretion and are not produced at high accretion rates (or are produced with low efficiency).

The problem of low radiative efficiency of disks is conventionally explained by accretion in ADAF mode. In the standard SS model, the accreting material is cooled efficiently. All the energy released through viscosity is radiated. The accreted gas is much cooler than the local virial temperature. The orbiting material has a vertical thickness much smaller than the radius. However, if the cooling is not able to keep up with the heating, then a part of the released energy will have to be advected with the accreted gas. The gas has a higher temperature, but lower luminosity than in the SS disks. The analysis of this kind of flow resulted in a model of geometrically thick but optically thin disks with suppressed bolometric luminosity of the disk [5]. In these disks, the height of the disk is of the order of the radius while the radial velocity of the accreted matter is higher than in the SS model. The density of matter in the disk appears much lower than in the SS disk. If the free–free processes dominate in the emissivity of the disk, this results in strong reduction of radiation from the disk. Only a small fraction of the released gravitational energy goes into radiation. ADAF is a very inefficient regime of accretion regarding transformation of the gravitational energy of the accreted material into radiation or energy of jets. The major part of the energy is advected into the black hole and goes into increasing of its mass.

However, ADAF does not solve the problem with energetics of jets. This model needs an additional source of energy to energize them. A rotating (Kerr) black hole can supply the jets by the energy of rotation. A Kerr black hole placed in an external magnetic field makes it co-rotate, producing an effect similar to the rotation of the pulsar magnetosphere. This results in an extraction of rotational energy and angular momentum from the black hole which is carried out by an electron–positron wind. This is the so called Blandford and Znajek effect [42]. Estimates made by Blandford and Znajek have shown that the energy of the outflow is small compared with the radiation from conventional SS disks. However, this is valid only if we consider moderate rotation and conventional values of the magnetic field according to the SS model. A new model of a Magnetically Arrested Disk (MAD) has been introduced in the work [43]. This model is based on the assumption that the interstellar magnetic field $\sim\mu G$ is dragged to the center by the converging accreting plasma like it was shown in [44] to the level where the magnetic field disrupts the disk. The value of the magnetic field in this case essentially exceeds the conventional magnetic field in SS disks. Numerical simulations in fully 3D geometry show that the energy flux in the outflow from the black hole can achieve a value of the order $3\dot{M}c^2$, provided that the black hole rotates close to the maximal possible angular momentum [45].

Thus, one of the possible models able to explain the energetics of accretion and outflow from AGN needs the following set of assumptions. It is necessary to assume that accretion occurs in the ADAF regime, that the main source of energy of jets is the energy of rotation of the black hole rotating close to the maximal limit and finally that accretion results in the formation of the Magnetically Arrested Disk (MAD) in its inner part. In this review, an alternative approach to the problem of disk accretion is discussed. In the alternative approach, the only available energy of AGNs including jets is the gravitational energy released in the accretion.

In conventional theories of disk accretion, turbulent viscous stresses provide loss of the angular momentum of the accreted matter. However, the angular momentum and rotational energy can be lost due to another mechanism. Wind from a rotating magnetized object can carry away its angular momentum and rotational energy. Starting with the classical work of Parker [46], it was clear that all main sequence stars, including the Sun, eject matter in the form of winds. Schatzman [47] proposed that as the winds contain a frozen-in magnetic field that goes back to the star, the angular momentum loss is leveraged many times. The importance of stellar winds in extracting angular momentum from main sequence stars was recognized by Mestel [48,49]. Pulsars also lose their energy of rotation due to a similar mechanism. The wind of electron–positron plasma produced in the pulsar magnetosphere carries out all the rotational energy of the pulsar. It is important to pay attention that the loss of the angular momentum is accompanied by a corresponding loss of the energy of rotation without essential heating of the stars and pulsars. In the case of accretion disks, we are sure that they produce outflows in the form of magnetized winds and jets. It is natural to assume that, in addition to the loss of the angular momentum due to the viscosity, the matter in the disk loses its angular momentum due to the magnetized wind. This idea was first formulated by Blandford and Payne [50]. Pelletier and Pudritz [51] pointed out that the loss of the angular momentum due to the wind can dominate over the loss of the angular momentum due to the viscosity under rather conventional conditions. Later, this idea has been explored in many works of the Grenoble group [52–55], which called this type of flow around black holes Magnetized Accretion–Ejection structures (MAES). Several other authors over the years explored similar approaches in different physical contexts [56–60]. In the last works of the Grenoble group [61,62], the radiation from the Jet Emitting Disks (JED) is discussed in the context of X-ray binaries. Starting with our first work [63] devoted to the same problem, we focused on the fact that these disks can be the key to the solution of the problem of high ratio of the kinetic luminosity of the jets over the bolometric luminosity of the disks. Actually, Ferreira and Pelletier [53,55] noted much earlier that, under conventional conditions, the jet can carry out almost all the angular momentum and energy from the accretion disk. Due to this, the radiation from the disk appears suppressed and we arrive to another model of a radiatively inefficient disk. However, unlike ADAF, in this case, the system black hole and the disk is a very efficient system. It transforms almost all the energy released at the accretion in to the kinetic energy of jets. In this case, we have $L_{kin}/L_{Edd} \approx \dot{m}$. No additional sources of energy are necessary.

The review is based mainly on the results obtained in the National Research Nuclear university (MEPHI), although a lot of results have been obtained earlier by the Grenoble Group (see Refs. [52–55]). We acknowledge this in the appropriate places.

## 2. Magnetic Field of the Disk and Wind

### *Assumed Structure of the Magnetic Field in the Disk*

In the case of ideal plasma (viscosity and electric resistivity are neglected), the magnetic field is determined by advection of the field lines by the accreted plasma to the center. This process was firstly considered in [64]. However, the matter in the disk is evidently not ideal. Turbulence produces rather strong turbulent viscosity and electric resistivity. Therefore, the processes of diffusion of matter across the magnetic field lines also take place in the disk. Moreover, the process of diffusion appears so strong that prevents accumulation of the magnetic flux at the central part of the accretion disk what makes the operation of the Blandford and Znajek effect problematic [65,66]. Some ideas about how to avoid this problem are discussed in [67,68].

The majority of the works devoted to the process of disk accretion consider the disk as a thin layer of plasma penetrated by the field lines of one polarity. The value of the magnetic field and magnetic field pressure is defined by two processes: by the process of advection of the field lines to the disk center and by the process of diffusion of the field lines in the opposite direction. Equilibrium of these processes provides a steady state structure of the magnetic field. This approach was used by the Grenoble group starting with work [52]. However, there is a general understanding that the process of disk dynamo plays a major role in the production of the magnetic field inside the disk [69–73]. In addition, a quite specific dynamo mechanism can operate in the disks [74,75], although they remain debatable [76].

The dynamo mechanism results in formation of small scale loops of the magnetic field which basically defines the viscosity of the matter of the disk. Numerical simulations show that the loops emerge on the surface of the magnetic field in accordance with the predictions made in [69], and expand into surrounding space at the differential rotation of the field line foot points in the disk [77,78]. Pressure of plasma and centrifugal forces leads to the opening of the field lines and to the formation of magnetized wind along open field lines. The schematic structure of the magnetic field lines inside and outside the disk is shown in Figure 1. It is reasonable to consider the disk with the wind in the quasi steady state. In this state, the average value $< B^2 >$ does not vary with time, while the time derivative $\frac{\partial \mathbf{B}}{\partial \mathbf{t}} \neq 0$. The average pressure of the magnetic field does not change with time, but the polarity of $\mathbf{B}$ varies with time, so that the average over time value of $\mathbf{B}$ is equal to zero. This is valid for the magnetic field inside the disk and for the magnetic field in the wind. The field lines of the wind of the opposite polarities are separated by current sheets. We assume that, like in the case of the Sun, the process of field annihilation due to field line reconnection in the current sheets takes place inside the disk and corona, while, in the wind, the activity of the current sheets in the wind is suppressed. Therefore, the dynamics of plasma in the current sheets can be considered in the ideal MHD approximation. All the dissipative processes connected with the final electric conductivity and viscosity are neglected. The current sheets in this approximation are MHD discontinuities with zero thickness. Observations of a fine structure of the magnetic field of the solar wind support this assumption. The small scale magnetic field of the coronal streamers produces multiple current sheets in the interplanetary space that are observed even at the Earth orbit [79,80].

In this picture, the magnetic field in the wind changes with time. Although the magnetic pressure can be constant in the steady state flow, the magnetic field permanently changes polarity because a new magnetic field emerges from the interior of the disk and advection replaces the field lines of one polarity with field lines of the opposite polarity. Nevertheless, the problem of the wind outflow with such a magnetic field can be reduced to the problem of the wind outflow in the unipolar magnetic field like it was done in the work [50].

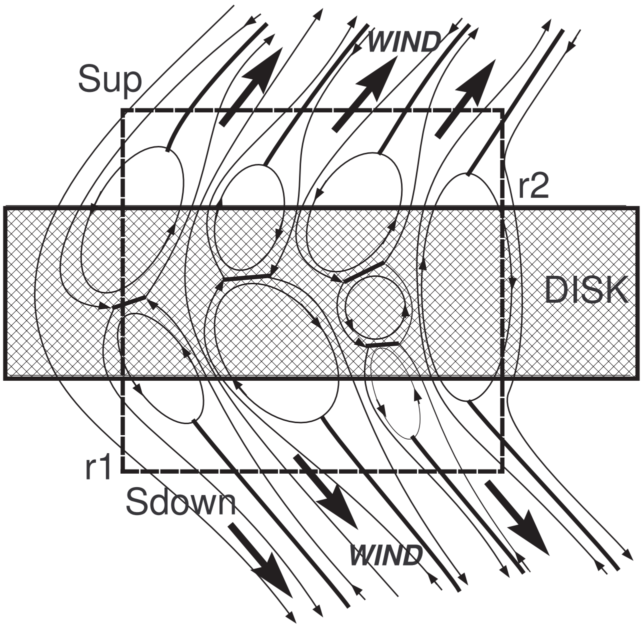


**Figure 1.** The structure of the magnetic field in the accretion disc and in the out flowing wind. The disc is shadowed. The magnetic field lines in the disc are distributed chaotically. At the base of the wind from the disc, all the magnetic field lines are opened. Their polarities are random. Therefore, the total magnetic flux leaving one side of the disc equals zero. The box drawn in dashed thick lines is the region of integration of conservation laws connecting the properties of the disc and the wind.

## 3. Basic Equations of the Accretion and Outflow

The flow in the disk has huge hydrodynamic and magnetic Reynolds numbers. This means that the viscosity and electrical conductivity are determined by turbulence. The collisional viscosity and electrical conductivity can be neglected. Therefore, we will start with the ideal plasma approximation. The condition of ideality has the form

$$\mathbf{E} + \frac{1}{c}\mathbf{v} \times \mathbf{B} = 0, \tag{1}$$

where $\mathbf{E}$ is the electric field, $\mathbf{B}$—magnetic field and $\mathbf{v}$ is the velocity of the plasma.

The dynamics of plasma is defined by the momentum conservation equation having the following form in the tensor representation [81]

$$\frac{\partial \rho v_i}{\partial t} + \frac{\partial \sigma_{ik}}{\partial x_k} = -\rho G M \frac{R_i}{R^3}, \tag{2}$$

where

$$\sigma_{ik} = \rho v_i v_k + p\delta_{ik} - \frac{1}{4\pi}(B_i B_k - \frac{1}{2}B^2 \delta_{ik}). \tag{3}$$

The second equation expresses the energy conservation in the form

$$\frac{\partial W}{\partial t} + \frac{\partial q_k}{\partial x_k} = 0, \tag{4}$$

$W = \rho e + \frac{B^2}{8\pi}$ is the sum of the thermal and magnetic field energy densities, and $e$ is the thermal energy per particle. We consider here only nonrelativistic flows. The term related to the electric field is omitted in $W$. The flux of the energy density equals

$$q_i = \rho v_i \left( w + \frac{v^2}{2} - \frac{GM}{R} \right) + \frac{c}{4\pi} [E \times B]_i + Q_i \,, \tag{5}$$

where $Q_i$ is the density of the energy flux of radiation.

In Cartesian coordinates, the angular momentum vector is introduced as $l_i = \varepsilon_{imp} x_m \rho v_p$ [82], where $\varepsilon_{imp}$ is the unit antisymmetric tensor. Application of this transformation to Equation (2) gives

$$\frac{\partial l_i}{\partial t} + \frac{\partial m_{ik}}{\partial x_k} = 0, \tag{6}$$

where $m_{ik} = \varepsilon_{imp} x_m \sigma_{pk}$. Projection of this equation on the $z$ axis gives

$$\frac{\partial l_z}{\partial t} + \frac{\partial m_{zk}}{\partial x_k} = 0, \tag{7}$$

where $l_z = \rho v_\varphi r$ and

$$m_{zk} = \rho v_k r v_\varphi - \frac{1}{4\pi} r B_k B_\varphi. \tag{8}$$

The conservation equations for the matter and the magnetic fluxes are

$$\frac{\partial \rho}{\partial t} + \frac{\partial \rho v_k}{\partial x_k} = 0, \tag{9}$$

and

$$\frac{\partial B_k}{\partial x_k} = 0. \tag{10}$$

These equations are supplemented by the equation of induction

$$\frac{\partial \mathbf{B}}{\partial \mathbf{t}} + \mathrm{curl}\mathbf{E} = \mathbf{0}. \tag{11}$$

## 4. Conservation Laws for the Disk

In this section, we obtain vertically integrated equations conventionally explored in the theory of accretion disks. We study a steady state axisymmetric accretion and outflow. Because of turbulent motion inside the disk, all variables vary in time on small time scales. Below, we consider equations for ensemble-averaged variables. The ensemble is the large number of identical accretion disks. In the steady state flow, these variables are constant in time. Averaging is expressed by the brackets $< ... >$. Application of the averaging operation to the terms in the equations with time derivatives makes them equal to zero.

Let us consider a control volume in the form of ring with rectangular cross section in the poloidal plane as it is shown in Figure 1. The cross section is shown with a thick dashed line. The control volume includes a fragment of the disk and corona. The upper and lower boundaries of the volume are located at the base of the wind above the disc. All the magnetic field lines of the wind are rooted here.

Integration of the equations over the control volume gives us the equations in integral form. Conservation of the angular momentum, energy and mass are as follows:

$$\oint_S < m_{zk} > dS_k = 0, \tag{12}$$

$$\oint_S < q_k > dS_k = 0, \tag{13}$$

$$\oint_S < \rho v_k > dS_k = 0. \tag{14}$$

Integration here is performed along a closed surface surrounding the volume. The surface consists of the sides $S_1$ at radius $r_1$, side $S_2$ at radius $r_2$ and upper and down sides $S_{up}$ and $S_d$. Integration gives

$$\begin{aligned} &-\int_{-h}^{h} r^2 < \rho v_\varphi v_r > dz\Big|_{r1} + \int_{-h}^{h} r^2 < \rho v_\varphi v_r > dz\Big|_{r2} \\ &+ \frac{1}{4\pi}\int_{-h/2}^{h} r^2 < B_r B_\varphi > dz\Big|_{r1} - \frac{1}{4\pi}\int r^2 < B_r B_\varphi > dz\Big|_{r2} \\ &+2\int_{r1}^{r2}\left(r < \rho v_\varphi v_z > -\frac{1}{4\pi} r < B_\varphi B_z >\right)_{S_{up}} r\,dr = 0. \end{aligned} \tag{15}$$

Integration across the disc is performed in the interval on $z$ from $-h$ to $h$ correspondingly at the radiuses r1 and r2. Integrations along $S_{up}$ and $S_d$ are equal to each other because the vector $d\mathbf{S}$ and the component of the velocity $v_z$ change sign simultaneously. Therefore, we simply double the integration along the surface $S_{up}$. This equation can be rewritten in the form

$$\begin{aligned} &-\int_{-h/2}^{h} r^2 < \rho v_r >< v_\varphi > dz\Big|_{r1} + \int_{-h/2}^{h} r^2 < \rho v_r >< v_\varphi > dz\Big|_{r2} \\ &-\int_{-h}^{h} r^2(< \delta\rho v_r \delta v_\varphi > -\frac{1}{4\pi} < B_r B_\varphi >)\,dz\Big|_{r1} + \int r^2(< \delta\rho v_r \delta v_\varphi > -\frac{1}{4\pi} < B_r B_\varphi >)\,dz\Big|_{r2} \\ &+2\int_{r1}^{r2}\left(r < \rho v_\varphi v_z > -\frac{1}{4\pi} r < B_\varphi B_z >\right)_{S_{up}} r\,dr = 0, \end{aligned} \tag{16}$$

where symbol $\delta$ means deviation of the value from average. The term

$$t_{\varphi r} = -(< \delta(\rho v_r)\delta v_\varphi > -\frac{1}{4\pi} < B_r B_\varphi >) \tag{17}$$

is the efficient viscosity of the matter caused by the turbulent motion and magnetic fields inside the disk.

Equation (16) is reduced to the differential form as follows:

$$\begin{aligned} &\frac{\partial}{r\partial r}\left(r^2(\int_{-h}^{h} V_k < \rho v_r > -t_{r\varphi})\,dz\right)|_{disc} \\ &+2r\left(< \rho v_\varphi v_z > -\frac{1}{4\pi} < B_\varphi B_z >\right)|_{wind} = 0. \end{aligned} \tag{18}$$

The subscripts $|_{disc}$ and $|_{winds}$ denote the variables describing the disc and the wind at the base (at the surface $S_{up}$). According to this equation, the angular momentum of the disc is carried out by the out flowing plasma and by the magnetic stresses in the outflow. Introducing the accretion rate in the disk as

$$\dot{M} = -2\pi r\int_{-h}^{h} < \rho v_r > dz, \tag{19}$$

we finally obtain for conservation of the angular momentum of the disk the following equation

$$\frac{\partial}{r\partial r}\left(rV_k\dot{M}+4\pi r^2 t_{r\varphi}h\right)|_{disc}$$
$$-4\pi r\left(V_k<\rho v_z>-\frac{1}{4\pi}<B_\varphi B_z>\right)|_{wind}=0. \tag{20}$$

Everywhere below, we accept that the azimuthal velocity of the plasma in the disc $<v_\varphi>=V_k$, where $V_k=\sqrt{GM/r}$ is the Kepler velocity and the disk is geometrically thin with aspect ratio $h/r<<1$. Similar manipulations with the energy conservation equation give the following equation

$$\frac{\partial}{r\partial r}\int_{-h/2}^{h} r\left(<\rho v_r w>+\frac{<v_r B^2>}{4\pi}+\frac{<\rho v_r v^2>}{2}-<\rho v_r>\frac{GM}{r}-\frac{<B_r(\mathbf{vB})>}{4\pi}+<Q_r>\right)dz|_{disc}$$
$$+2\left(<\rho v_z\left(\frac{w+v^2}{2}-\frac{GM}{R}\right)>+\frac{c}{4\pi}<[E\times B]_z>+Q_z\right)|_{wind}=0. \tag{21}$$

In this equation, the term $<\rho v_r\frac{v^2}{2}>$ can be expanded as

$$<\rho v_r v^2>=<\rho v_r V_k^2>+<\rho v_r 2V_k\delta v_\varphi>+<\rho v_r\delta v_\varphi^2>+<\rho v_r^3>+<\rho v_r v_z^2>, \tag{22}$$

taking into account that $V_k\gg\delta v_\varphi$, $V_k\gg\delta v_z$ and $V_k\gg\delta v_r$, we remain with

$$<\rho v_r v^2>\approx<\rho v_r>V_k^2+2V_k<\rho v_r\delta v_\varphi>. \tag{23}$$

Starting at Ref. [3], it is assumed that the energy density of the chaotic magnetic field in the disk is of the order of density of the turbulent energy, $\rho v_t^2/2\sim B^2/4\pi$. Both of them are much less than $\rho V_k^2/2$. These terms are also omitted in Equation (21). The term $<B_r(\mathbf{vB})>$ is expanded into

$$<B_r(\mathbf{vB})>=<B_r^2 v_r>+<B_r B_\varphi>V_k+<v_z B_z B_r>. \tag{24}$$

The term $<B_r B_\varphi>V_k$ is much larger than the remaining. We neglect them. For the same reasons,

$$<\rho v_z(\frac{w+v^2}{2})>\approx<\rho v_z>\frac{V_k^2}{2}. \tag{25}$$

The $z$ component of the Poynting flux

$$<[E\times B]_z>=<E_r B_\varphi>-<E_\varphi B_r>, \tag{26}$$

where $E_r=\frac{1}{c}(v_z B_\varphi-v_\varphi B_z)$ and $E_\varphi=\frac{1}{c}(v_r B_z-v_z B_r)$. Keeping in Equation (26) the largest term, we obtain that

$$<[E\times B]_z>\approx-\frac{V_k}{c}<B_z B_\varphi>. \tag{27}$$

After substitution of all these equations into Equation (21) taking into account Equations (30) and (19), we obtain the equation expressing energy conservation in the disk

$$\frac{1}{r}\frac{\partial}{\partial r}\left(\dot{M}(\frac{V_k^2}{2}-\frac{GM}{r})+4\pi rV_k t_{r\varphi}h\right)_{disc}$$
$$-4\pi\left(<\rho v_z>\left(\frac{V_k^2}{2}-\frac{GM}{R}\right)-\frac{V_k}{4\pi}<B_\varphi B_z>+Q_z\right)_{wind}=0. \tag{28}$$

The last equation is the matter conservation

$$\frac{\partial}{r\partial r}\left(r\int_{-h/2}^{h}\rho v_r\,dz\right)_{disc}+(2\rho v_z)_{wind}=0. \tag{29}$$

Exploring definition (19), the last equation takes the form

$$\frac{\partial \dot{M}}{\partial r}-4\pi r\rho v_z=0. \tag{30}$$

Subtraction from Equation (28) of Equation (20) multiplied with the Keplerian angular velocity $\Omega_k = V_k/r$ results in the energy flux of radiation from one side of the surface of the disk being

$$Q = Q_z = t_{r\varphi} r h \frac{\partial \Omega_k}{\partial r} \tag{31}$$

like in the classical accretion disk of Shakura and Sunyaev [3]. Below, instead of $Q_z$, we will use $Q$.

## 5. The Problem of the Wind Outflow

### 5.1. Invariance Principle

Below, we consider only axisymmetric flows when all the averaged variables do not depend on the azimuthal angle. In this case, the problem of the wind outflow can be essentially simplified. However, the problem of the plasma outflow in the poloidal magnetic field which changes polarity remains too complicated. This problem can be simplified by reduction to the same problem in the unipolar magnetic field.

It follows from equations of ideal MHD that the dynamics of plasma in ideal MHD is invariant in relation to a reversal of the direction of the magnetic field lines in an arbitrary flux tube. This property of ideal MHD flows was used for the solution of the problem of plasma outflow from pulsars [83]. This property was called the invariance principle.

The plasma flow in the nonrelativistic limit is described by the set of ideal MHD Equations (1), (2), (4), (7) and (9)–(11).

Let us assume that we have some solution which is described by the functions $\mathbf{B}(r,t)$, $\rho(r,t)$, $\mathbf{V}(r,t)$ and $P(r,t)$. It is easy to show that changing of polarity of the magnetic field ( and corresponding electric field) in an arbitrary flux tube does not change dynamics of plasma.

Let us introduce a scalar function $\eta(r,t)$ with the property that $\eta = 1$ everywhere except inside the chosen flux tube where $\eta = -1$. This function satisfies the following two conditions:

$$\mathbf{B}\cdot\nabla\eta = 0, \tag{32}$$

and

$$\frac{\partial \eta}{\partial t}+\mathbf{V}\cdot\nabla\eta = 0. \tag{33}$$

The second equation is the consequence of Equations (1), (11) and (32). The value of $\eta$ is advected together with the plasma.

Then, the solution $\eta\mathbf{B}(r,t)$, $\rho(r,t)$, $\mathbf{V}(r,t)$ and $P(r,t)$ also satisfies the system of Equations (1), (2), (4), (7) and (9)–(11). Indeed, the tensor of the momentum flux density (3) is bi quadratic in relation to the magnetic field. It does not change because $\eta^2 = 1$. This means that the forces affecting the plasma do not change with this transformation.

Let us consider how this principle operates in the most simplified model of the wind outflow from the surface of a star. The distribution of the normal component of the poloidal magnetic field is axisymmetric. In that case, we get the model with the axisymmetric wind. According to the invariance principle, the change of the direction of magnetic field lines in some flux tube does not affect the dynamics of the plasma. Let us assume that we obtain a solution for the axisymmetric rotator, as shown schematically in Figure 2a. Then, a reversal of the sign of some magnetic field lines in an arbitrary poloidal flux tube gives us a solution which is not axisymmetric and non stationary, as shown in Figure 2b. This is a solution for the plasma outflow from a rotator with axisymmetric $B^2$ at the surface but with a magnetic spot of the opposite polarity on the upper hemisphere. Figure 2b shows the cross-section of such a magnetic field by the poloidal plane. The stream lines are the same as for the axisymmetric case. However, the poloidal magnetic field changes sign in the magnetic spot corresponding to the flux tube of the opposite polarity. The path of the field line in this flux tube in 3D is shown by a dashed line. These spots propagate in the poloidal plane with the velocity of the plasma and hence the pattern is non stationary. It is clear that the number of such magnetic spots and their position at the base surface can be arbitrary.

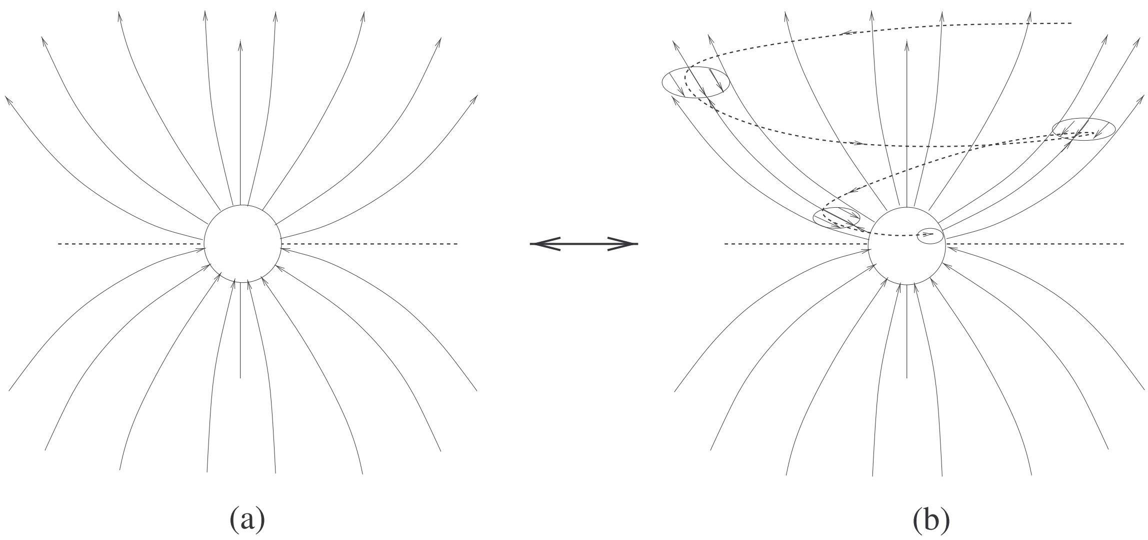


**Figure 2.** Plasma flow from an axisymmetric rotator with an initially split-monopole magnetic field, as in (**a**). Reversing the direction of the poloidal magnetic field in an arbitrary flux tube does not change the dynamics of the problem while we obtain the configuration shown in (**b**) which describes a non stationary and nonaxisymmetric plasma flow from a rotator with a magnetic spot of opposite polarity on the base surface. The distribution of such spots can be arbitrary.

Now, let us return to the accretion disk. In our model, the accretion disk can be considered as a layer at the equatorial plane with thickness $2h$. All magnetic field lines are open and chaotically change polarity in the wind. The total magnetic flux penetrating in to the disk equals zero. This means that the disk brings to the black hole zero total magnetic flux. The formation of such a wind has been investigated numerically in [78]. This naturally solves the old problem which was pointed out in the first works on the accretion of the magnetized plasma [44,64]. The magnetic flux of one polarity can be accumulated at the center preventing the accretion. There is no chance to annihilate this flux due to magnetic field reconnection. In our case, the situation changes dramatically. The magnetic flux can fully annihilate near the black hole, where the geometrical scales become much smaller in comparison with scales in the disk because the plasma is filled by a large amount of current sheets separating flux tubes of opposite polarities. Reconnection of the field lines near the black hole horizon can be accompanied by the sporadic ejection of mass of plasma.

The invariance principle allows us to essentially simplify the solution of the problem of the wind outflow from the disk. According to this principle, we can replace the direction of all the field lines making them unidirectional in every hemisphere. The dynamics of the wind does not change. After that, we arrive to the wind outflow in the unidirectional magnetic field like in the pioneering work by

Blandford and Payne [50]. This procedure is shown in Figure 3 and corresponds to the transition from the upper to the lower panel.

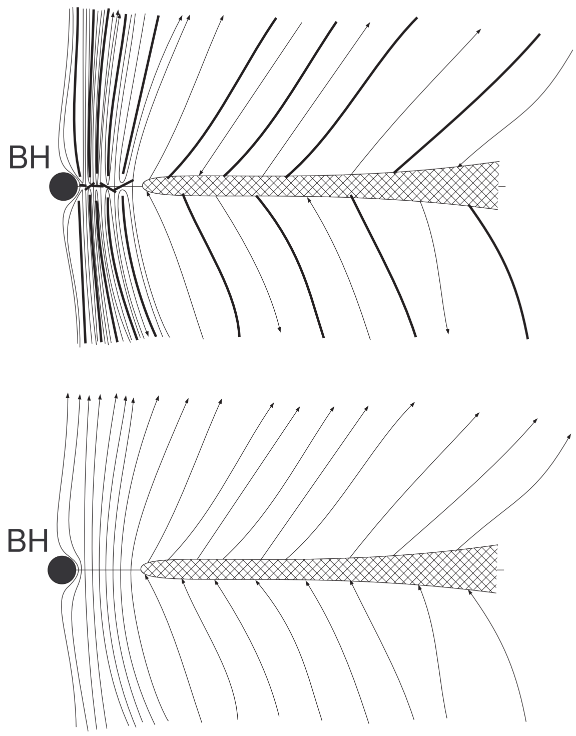


**Figure 3.** The **upper** panel shows the structure of the magnetic field outside the disk. The magnetic field lines (thin lines) leaving the disk from both sides chaotically change polarity. The flux tubes of opposite polarities are separated by the current sheets (thick lines). This system of field lines is compressed at the black hole horizon where an efficient reconnection takes place annihilating the magnetic field. The replacement of the magnetic field lines leaving the disk by the similar lines of one polarity does not change the dynamics of the wind and satisfy Maxwell's equations. This allows us to use the model shown in the **lower** panel where the magnetic field is unipolar.

### *5.2. The Role of the Azimuthal Electric Field in the Wind*

In the limit of axisymmetric flow in the unipolar magnetic field, the azimuthal component of Equation (11) and the frozen-in condition (1) for the same component give a couple of equations

$$\frac{\partial}{\partial r}(rE_\varphi) = 0, \tag{34}$$

and

$$E_\varphi + \frac{1}{c}\left(v_z B_r - v_r B_z\right) = 0. \tag{35}$$

The solution of Equation (34) results in

$$E_\varphi = \frac{A}{r}, \tag{36}$$

where $A$ is some constant. This solution diverges at $r \to 0$. It was pointed out in [84] that $E_\varphi$ is not equal to zero at the accretion of an ideal plasma onto a gravitating center. Indeed, as it follows from Equation (35), $E_\varphi$ at the base of the wind is equal to $\frac{1}{c}v_r B_z$ provided that $v_z \to 0$ at the center of the disc. At accretion $v_r \neq 0$, there is thus $E_\varphi \neq 0$ as well. Thus, in the region of the accretion flow, $E_\varphi$ can not be neglected because it is connected directly with the radial velocity of the plasma in the disc.

As it follows from Equation (35) in this case, the velocity has a poloidal component $v_\perp$ orthogonal to the poloidal magnetic field line. The plasma in the wind is advected to the center together with the matter in the disk. Nevertheless, this component of the electric field can be neglected when we consider the dynamics of the wind under the condition $v_\perp \ll v$, where $v$ is the full velocity of the plasma. If we take into account that $v \sim V_k$ and that $v_\perp = c\,\frac{E_\varphi}{B_p}$ the toroidal electric field can be neglected under the condition

$$\frac{B_{p0} r_0^2}{B_p r^2} \frac{v_r(0) r}{V_k r_0} \ll 1. \tag{37}$$

The value $B_p r^2$ roughly equals the full flux of the magnetic field through the surface limited by the field line. It can not change strongly along the field line, $\frac{B_{p0} r_0^2}{B_p r^2} \sim 1$. Therefore, inequality (37) is inevitably violated at the distance $r \gg r_0 \frac{V_k}{v_r(0)}$. However, we do not care about validity of Equation (37) in all of space.

In order to take into account the impact of the wind on the process of accretion, it is necessary to calculate the product $B_z B_\varphi$ at the base of the flow. The flow of the wind does not depend on the conditions down stream, the so called fast mode surface where the velocity of plasma equals the fast mode magnetosonic velocity. To be more exact, this should be called the fast mode separatrix surface [85]. However, the difference between them is not important for us here. Thus, the product $B_z B_\varphi$ at the base of the wind is determined by the flow in the zone limited by the fast mode surface. Therefore, the toroidal electric field in the wind can be neglected if

$$\frac{v_r(0) R_F}{V_k r_0} \ll 1, \tag{38}$$

where $R_F$ is the radius of the fast mode surface.

This condition can be understood from another point of view. The equilibrium state in the zone limited by the fast mode surface is formed during the time an MHD signal spends for travel from the base to the fast mode surface $\sim R_F/V_F$, where $V_F$ is the fast mode velocity that is close to the Alfven velocity at the Alfven surface. At the Alfven surface, the velocity of plasma is $\sim V_k$. The impact of the advection of the matter in the disk on the dynamics of the wind can be neglected if the root of the magnetic field line is displaced over the distance $\Delta r \ll r_0$ during this time. In this case, we arrive at the same Equation (38).

### *5.3. Along Field Line MHD Equations of the Wind*

If the azimuthal electric field can be neglected, $E_\varphi = 0$, then, according to Equation (35), the poloidal velocity is directed along the poloidal magnetic field. In this case, we have

$$l_p = \rho r v_p \left( v_\varphi - \frac{B_p}{4\pi\rho v_p} B_\varphi \right), \tag{39}$$

for the angular momentum flux density along a poloidal filed line and

$$q_p = \rho v_p \left( \frac{v^2}{2} - \frac{GM}{R} - \Omega r \frac{B_p}{4\pi\rho v_p} B_\varphi \right) \tag{40}$$

for the energy density flux along a poloidal field line. If we take into account that the fluxes of the angular momentum $lpdS$, energy $q_p dS$, matter $\rho v_p$ and magnetic field flux $B_p dS$ are conserved as it is demonstrated in Figure 4, it can be obtained that the following two integrals of motion take place along the field lines

$$r v_\varphi - \frac{r B_p B_\varphi}{4\pi\rho v_p} = L, \tag{41}$$

and

$$\frac{v^2}{2} - \frac{GM}{R} - \Omega\frac{rB_pB_\varphi}{4\pi\rho v_p} = H. \tag{42}$$

The first equation from this couple is the conservation of the angular momentum per particle $L$ and the second one is the conservation of the energy per particle $H$ along a field line.

An additional consequence from $E_\varphi = 0$ is that the poloidal electric field $E_p$ is perpendicular to the poloidal magnetic field $B_p$. In this case, Equation (11) gives that the product $E_p dl$ is conserved along a field line, where $dl$ is the distance between two neighbor field lines. If we take into account that $dS = 2\pi r dl$, we obtain that $E_r = -r\Omega B_z/c$ and $E_z = r\Omega B_r/c$ or $E_p = \frac{r\Omega}{c}B_p$. The frozen-in condition for the poloidal component of the electric field gives in this case that

$$r\Omega B_p + v_p B_\varphi = v_\varphi B_p. \tag{43}$$

Combining Equation (43) with Equation (41) results in

$$rv_\varphi = \frac{L - r^2\Omega\frac{B_p^2}{4\pi\rho v_p^2}}{1 - \frac{B_p^2}{4\pi\rho v_p^2}}. \tag{44}$$

The denominator of this expression goes to zero at the Alfvenic point where $v_p = B_p/\sqrt{4\pi\rho}$. The nominator of this expression must equal to 0 in this point to provide regularity of $v_\varphi$. From this condition, we obtain that the momentum per particle equals $L = \Omega r_A^2$, where $r_A$ is the cylindrical radius at the Alfvenic point where the plasma velocity equals the local Afvenic velocity $V_A = \sqrt{B_p/4\pi\rho}$.

Taking into account that $B_p/v_p = B_z/v_z$ in the wind, it is easy to determine that the product

$$rB_zB_\varphi = -4\pi\rho v_z\Omega_k r_0^2(\lambda - 1), \tag{45}$$

at the base of the wind located at the radius $r_0$. Following [54], $\lambda = r_A^2/r_0^2$.

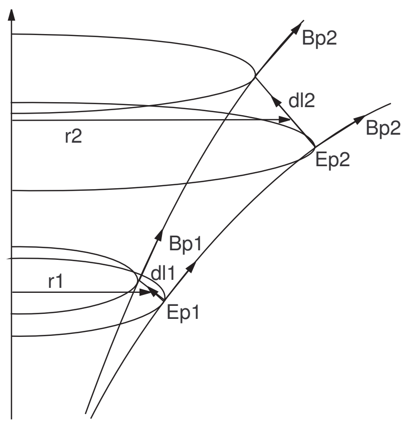


**Figure 4.** Fluxes of the magnetic field, matter, energy and angular momentum between any two close field lines with the cross section $dS = 2\pi r dl$ are conserved. The condition curl $\mathbf{E} = \mathbf{0}$ gives that the product $E_p dl$, where $dl$ is the distance between these field lines is also conserved.

## 6. Disk-Wind Connection at the "Cold" Accretion

Taking into account the equation for mass conservation (30), the equations for angular momentum conservation can be rewritten in the form

$$\dot{M}\frac{\Omega_k}{2} + \frac{1}{r}\frac{\partial}{\partial r}\left(4\pi r^2 t_{r\varphi} h\right)|_{disc}$$
$$+r < B_\varphi B_z > |_{wind} = 0. \tag{46}$$

The energy conservation is fulfilled automatically provided that Equation (31) takes place. It follows from Equation (46) that the impact of the wind on the dynamics of the wind is reduced to the value of $B_\varphi B_{z,wind}$. We omit here brackets $<>$ because in the steady state axisymmetric wind $B_\varphi B_{z,wind}$ is constant.

Taking into account Equation (45), Equation (46) can be rewritten in the form

$$\dot{M}\frac{\Omega_k}{2} + \frac{1}{r}\frac{\partial}{\partial r}\left(4\pi r^2 t_{r\varphi} h\right)|_{disc}$$
$$-4\pi\rho v_z \Omega_k r_0^2(\lambda - 1) = 0. \tag{47}$$

This equation clearly demonstrates that every particle of the wind carries out an amount of the angular momentum per particle equal to $\Omega_k r_0^2(\lambda - 1)$. In the case of purely hydrodynamical wind ($\mathbf{B} = \mathbf{0}$), this value equals 0 because $\lambda = 1$. The wind does not carry out any angular momentum from the disk. The magnetic field dramatically changes the situation. Thanks to it, $\lambda > 1$ and every particle of the wind carries out not only its own angular momentum, but also some fraction of the angular momentum of the particles remaining in the disk. A natural question arises. At what conditions does the wind carry out more angular momentum than it is transported outward by the viscous stresses?

As it was pointed out by [51], the momentum loss due to the wind will dominate the losses caused by the viscous stresses provided that

$$4\pi r t_{r\varphi} h \ll r^2 < B_\varphi B_z > |_{wind}. \tag{48}$$

In the opposite case, we have the standard SS version of the disk accretion [3].

The physical sense of inequality (48) becomes clear if we note that according to the assumptions of [3] and recent numerical simulations of the magnetic field generation [72]

$$-t_{r\varphi} \sim \frac{B^2_{disk}}{4\pi}, \tag{49}$$

where the magnetic field $B_{disk}$ is taken inside the disk. We distinguish the magnetic field inside the disk from the magnetic field at the base of the wind. In the works of the Grenoble group [53,54] and other authors [58–60], these values are similar because the magnetic field vertically crosses the disk. In reality, the magnetic field inside the disk can essentially exceed the field at the base of the wind [72]. The regime of "cold" disk accretion occurs when

$$\frac{\theta h}{r} \ll 1, \tag{50}$$

where

$$\theta = \frac{4\pi t_{r\varphi}}{< B_\varphi B_z > |_{wind}} \sim \frac{B^2_{disk}}{B^2_{wind}}. \tag{51}$$

For the geometrically thin disks with $h/r \ll 1$, "cold" disk accretion certainly has room for existence provided that $\theta$ is not extremely large.

Dissipative terms defined by $t_{r\varphi}$ can be neglected in Equations (28) and (46) in the regime of cold accretion. The equations for the angular momentum and energy conservation take the form

$$\dot{M}\frac{\Omega_k}{2} + r < B_\varphi B_z > |_{wind} = 0, \tag{52}$$

$$\frac{1}{2}\frac{\partial V_k^2 \dot{M}}{\partial r} + 4\pi r \rho v_z H|_{wind} = 0. \tag{53}$$

The luminosity of the disk is determined by Equation (31).

Our approach to the problem of disk accretion due to the wind methodologically differs from the approach used by the Grenoble group and other researchers. In the works of the Grenoble Group, the accretion and outflow are considered as one self-consistent process using a self similarity prescription. It was named Magnetized Accretion-Ejection structures (MAES) [52]. The advantage of this approach is that, simultaneously with the solution of the problem of accretion, the structure of the disk is determined. However, this is simultaneously a disadvantage because it is necessary to strongly simplify the processes in the disk and neglect for example dynamo processes and remain in the frameworks of self similarity prescriptions. Keeping in mind practically the same physical picture, we follow another methodology. We separate the problem of accretion from the problem of internal structure of the disk. The arguments in favor of this approach are the following.

The rate of the angular momentum loss by the disk due to the wind is determined by the product $B_z B_\varphi$ at the surface of the disk or, equivalently, at the base of the wind. It is known from the theory of MHD winds that, in order to solve the problem of the magnetized wind outflow from the surface of the rotating object (in our case the surface of the disk), it is necessary to specify a certain number of boundary conditions at the base of the wind [83]. At the base of the wind, the magnetic field pressure dominates the gas pressure, $v_s \ll V_A$, where $v_s$ and $V_A$ are the sound and Alfvenic velocities. Therefore, it is natural to assume that $V_A > v_z > v_s$. This means that the mass flux density should be specified as the boundary condition [83]. In addition, we have to specify as boundary conditions the temperature of the plasma, the pressure, the normal component of the magnetic field $B_z$ and the rotational velocity of the object—five parameters in total. It is remarkable that the toroidal component of the magnetic field $B_\varphi$ is determined from the solution of the problem of the wind outflow. This means that the angular momentum loss of the disk can be determined by solving the problem of the wind outflow only at the specified mass flux density distribution in the wind, temperature of the plasma, pressure, and $B_z$ at the base of the wind.

To determine these parameters, it is necessary to solve the problem of the internal structure of the disk. At present, no convincing solution of this problem is obtained. Therefore, it is reasonable to consider the disk as a layer which provides us, due to some processes, five parameters at the surface, which are the functions of the coordinate at the disk surface. In the case of cold accretion, these parameters reduce to two unknown parameters because temperature and pressure at the base of the wind can be taken equal to 0 because, at the base, the gas pressure is much lower than the magnetic field pressure. This is a so called cold wind. The angular velocity equals the Keplerian velocity of the disk. We remain with two unknown functions: $\rho v_z$ and $B_z$, which can be specified at the base of the wind as boundary conditions for the problem of the wind outflow. Below, we will see that, in the fully self-consistent solution, $\rho v_z$ can not be an arbitrary function. This function is defined by the distribution of $B_z$ over the disk surface at the fixed $\dot{M}$ at the inner edge of the disk. Thus, the process of cold accretion actually depends only on $\dot{M}$ at the inner edge of the disk and the distribution of $B_z$ over the surface of the disk.

The magnetic field at the surface of the disk is evidently limited from below. Our numerical modeling of the self-consistent disk outflow shows (see below) that $B_\varphi \sim B_z$ at the base of the wind.

In this case, the disk accretion is possible if the magnetic field at the surface of the disk satisfies the inequality

$$B_z^2|_{wind} > \frac{\dot{M}\Omega_k}{2r}. \tag{54}$$

*Basic Properties of the "Cold" Accretion*

Equation (47) can be rewritten in the form

$$\frac{\partial}{\partial r}(rV_k\dot{M}) - \frac{\partial \dot{M}}{\partial r} r_A(r)^2\Omega_k(r) = 0, \tag{55}$$

where $r_A(r)$ is the Alfven radius of the force line rooted into disc at the point with radius $r$. The solution of Equation (55) gives

$$\dot{M} = \dot{M}_{edge} \exp \int_{r_{in}}^{r} \frac{dr}{2r(\lambda(r) - 1)}, \tag{56}$$

where $\dot{M}_{edge}$ is the accretion rate at the inner radius of the disc $r_{in}$.

Equation (53) also can be rewritten in the following form. Using Label (30), it is easy to obtain that

$$\frac{\partial}{\partial r} \left.\frac{\dot{M}V_k^2}{2}\right|_{disc} + \frac{\partial \dot{M}}{\partial r} H_{wind} = 0. \tag{57}$$

We are interested in the solutions that allow particles to go to infinity from the disc. The necessary condition for this is $H > 0$. This condition means that the energy per particle is positive. This is necessary (but not sufficient) in order to have positive $v^2$ at a large distance from the source. The substitution of the explicit dependance (56) for $\dot{M}$ into Equation (57) results in

$$H = (2\lambda - 3)\frac{GM}{2r} = (2\lambda - 3)\frac{V_k^2}{2}. \tag{58}$$

This means that "cold" disk accretion is possible only at the magnetic field which satisfies the condition $\lambda > 3/2$ first obtained in [50]. Equation (58) shows also that the energy of a particle in the wind can essentially exceed the virial energy of the particle in the disk. Potentially, this fact gives us the key to the solution of the problem of large Lorentz factors of the jets from AGNs. Kinetic energy of the particles in the jets evidently strongly exceeds the virial energy of the particles at the last stable orbit of the disk.

## 7. Self-Consistent Solution of the Problem

To make sure that the model of "cold" accretion can reproduce real processes of the disk accretion onto a black hole, we have to obtain a convincing solution of the problem of self-consistent "cold" accretion and to verify whether this model can give a ratio of the kinetic luminosity of jets over the bolometric luminosity of the disk compatible with observations.

A lot of results in this regard have been obtained by the Grenoble Group. They used a self-similar prescription of the solution and considered the problem of the disk structure, accretion and outflow unified. The self-similarity imposes on the physics of the disk some extra demands, which do not satisfy the full set of equations. Nevertheless, solutions obtained by the Grenoble Group support the assumption that the process of accretion when the majority of the angular momentum of the accreted material is carried out by the wind can be realized indeed [54].

To obtain solutions beyond the self-similarity limitations, we use another approach. As we already discussed, we avoid consideration of the processes inside the disk. The disk is considered as a layer with the zero thickness. The processes inside the disk provide the boundary conditions at the base of the wind mass flux density $\rho v_z$ and magnetic field flux $B_z$. Self-consistency of the outflow and accretion means that the equation for mass conservation (30) and the equation for angular momentum conservation (52) are solved together with the full system of Equations (1), (2), (4), (7) and (9)–(11) defining the flow of the wind from the disk. Below, we present in short the basic properties of solution of the self-consistent problem in the self similar approximation and the numerical solution of the problem without self similarity assumptions.

*7.1. Basic Properties of Self Similar Solutions*

The most comprehensive study of types of self similar flows has been investigated by the Grenoble group [54]. The self similarity in the form proposed initially by [50] is used. In this kind of self similarity, all the variables depend on the coordinates in the form

$$G(z,r) = r^{\delta}\tilde{G}\left(\frac{z}{r}\right), \tag{59}$$

where $z, r$ are the cylindrical coordinates, and $\delta$ is the self similarity index.

The steady-state equations for an ideal, cold plasma (with pressure $p = 0$) (4), (7), (9)–(11) can be rewritten in vector form as

$$\rho(\mathbf{v}\nabla)\mathbf{v} = -\frac{1}{8\pi}\nabla\,\mathbf{B}^2 + \frac{1}{4\pi}(\mathbf{B}\nabla)\mathbf{B} - \rho\,\frac{GM\mathbf{R}}{R^3}\,. \tag{60}$$

According to the self similarity assumption, all the variables in these equations can be presented as

$$\begin{aligned} \mathbf{v}(r,z) &= r^{-\delta_v}\tilde{\mathbf{v}}(z/r), \\ \rho(r,z) &= r^{-\delta_\rho}\tilde{\rho}(z/r), \\ \mathbf{B}(r,z) &= r^{-\delta_B}\tilde{\mathbf{B}}(z/r). \end{aligned} \tag{61}$$

This representation of the variables says that they are scaled as the power law of $r$ and all functions depend on the angle $\xi$ defined as $\tan\xi = z/r$.

The superscripts $\delta_v$, $\delta_\rho$, and $\delta_B$ are determined from the following conditions. Substituting of Equations (61) into Equation (60) leads to the equations

$$2\delta_B - \delta_\rho = 2\delta_v = 1. \tag{62}$$

It follows from them that

$$\begin{aligned} \mathbf{v}(r,z) &= r^{-1/2}\,\tilde{\mathbf{v}}(z/r), \\ \rho(r,z) &= r^{-\delta}\tilde{\rho}(z/r), \\ \mathbf{B}(r,z) &= r^{-\frac{(1+\delta)}{2}}\,\tilde{\mathbf{B}}(z/r). \end{aligned} \tag{63}$$

It is evident that, in the self similar solution, $\lambda$ is constant for all field lines. According to Equation (56) the accretion rate in the disc varies with $r$ as follows:

$$\dot{M} = \dot{M}_{edge}\left(\frac{r}{r_{in}}\right)^{\frac{1}{2(\lambda-1)}}. \tag{64}$$

This dependence was explored first in [52]. The combination $1/2(\lambda-1)$ was called the ejection index. Substitution of (64) into (30) taking into account (63) gives the following relationship between $\lambda$ and $\delta$

$$\delta = \frac{3}{2} - \frac{1}{2\,(\lambda-1)}, \tag{65}$$

which has been first used in the work [54]. $\lambda$ can change from $\frac{3}{2}$ up to $\infty$. It is interesting that at the same time the index of self similarity varies only in the limits between $\frac{1}{2}$ and $\frac{3}{2}$.

It is interesting to compare this solution [63] with the classical solution of Blandford and Payne [50]. Their solution was not self-consistent. Equations (52) and (30) were not used. Therefore, index $\delta$ is not connected with $\lambda$ by Equation (65). The scaling of the magnetic field and density was taken in the form $B \sim r^{-5/4}$, $\rho \sim r^{-3/2}$ arbitrary as one of the possible scalings. The self similar solution for "cold" accretion reproduces the solution of Blandford and Payne with additional connection expressed by Equation (65). The scaling of the magnetic field depends on $\lambda$ as $B \sim r^{-(5/4-\frac{1}{2(\lambda-1)})}$ and density as $\rho \sim r^{(-\frac{3}{2}-\frac{1}{2(\lambda-1)})}$. It is interesting to point out that observations show that the density of plasma in real objects is more likely scaled with an index less than 3/2 [86], which can be explained by the fact that $\lambda \neq \infty$ or by deviation of the flow from self similarity.

There is another interesting result obtained in [63]. The solutions at relatively low $\lambda = 25$ in [63] and $\lambda = 30$ in [50] are quite similar. All flow lines diverge from the axis experiencing slight collimation. However, already at $\lambda = 64$, the solution obtained in [63] demonstrates perfect cylindrical collimation of the flow to the rotational axis at a rather large distance from the disk. It would be important to verify this result in the numerical solutions. This is one of the reasons why the numerical solutions of this problem are of special interest for us.

### *7.2. Numerical Solution of the Self-Consistent Problem*

In the numerical self-consistent solution, the equations for the mass and angular momentum conservation ((30), (52)) are solved together with the full system of Equations (1), (2), (4), (7), (9)–(11) determining the flow of the wind from the disk.

The problem of the flow of the wind is solved numerically by the method of relaxation explored practically in all the numerical solutions of the problems of the wind outflow from astrophysical objects. The dimension of the box of the numerical simulation was ($1000 \times 800$) expressed in gravitational radius $r_g = \frac{2GM}{c^2}$ and is located above the equatorial plane. The disk and plasma are assumed to be cold. The disk is located in the equatorial plane in the interval from 3 to 300 $r_g$. The verification of the solution and details of the solution of the problem by the relaxation method are presented in work [87]. Here, we focus on how to specify the boundary conditions at the disk in order to satisfy Equations (52) and (30).

The basic steps of the solution of this problem are the following. Firstly, we specify the distribution of $B_z$ over the surface of the disk from Equation (54) as

$$B^2_{z,min} = \frac{1}{2}\frac{\dot{M}\Omega_k}{r}. \tag{66}$$

For the calculations, we take the field three times higher than defined by (66).

After that, we specify the mass flux density $j = \rho v_{z,0}$ at the disk surface. The flow from the disk is sub Alfvenic. The initial velocity of the plasma is below the local Alfvenic velocity. The initial velocity at the disk is taken equal to $v_{z,0} = 0.01 \cdot V_k$. The density in this case is equal to $\rho_0 = j/v_{z,0}$. Equation (30) gives us the distribution of the mass loss rate along the radius of the disk $r$. However, we do not know what will be the product $B_{z,0}B_{\varphi,0}$ at the disk surface. While $B_z$ is specified at the disk, the component of the magnetic field $B_{\varphi,0}$ is defined from the solution of the problem of the wind outflow in all the computational domain. We stress that the product $B_z B_{\varphi,0}$ is not a simple function of $j$. It depends on the distribution $j$ over all the disk rather than on the value of $j$ at the same point. Moreover, even if the solution of the problem of the wind outflow is solved, the obtained distribution $B_{z,0}B_{\varphi,0}$ will not satisfy the equation for angular momentum conservation (52). The solution is not self-consistent in this case.

We propose the following iterative procedure [88].

1. The mass flux at the inner edge of the disk $\dot{M}_{edge}$ is specified and kept constant during the modeling;
2. The initial distribution of the mass flux $\dot{M}_n(r)$ as a function of $r$ is assumed. This is the iteration number $n = 0$. The most simple assumption at $n = 0$ is $\dot{M}_n(r) = \dot{M}_{in}$. Thus, $\dot{M}_0(r)$ is constant.

3. The initial distribution of the mass flux from the disk $(\rho v_z)_n$ is specified. At $n = 0$, the distribution of $(\rho v_z)_n$ is not connected with the accretion rate and the solution of the problem of the wind outflow is not self-consistent with the process of accretion.
4. Internal iterations are performed. The objective of the internal iteration is to define the distribution of $j$ which fulfills the angular momentum Equation (52).They are indexed by an additional index $k$. Therefore, the mass flux from the disk depends on two indexes and takes the form $j_{n,k}$. At every step $k$, the problem of the wind outflow is solved in all of the computational domains. The steady state solution is obtained and thus we obtain new value of $B_z B_\varphi$ at the disk surface. Of course, this value does not satisfy Equation (52) for the specified $\dot{M}_n$. Here, we make the next step of the internal iterations according to the following procedure. Let us introduce function

$$\Phi_k = -2r^{5/2} B_z B_\varphi \tag{67}$$

specified at the disk surface exploring the steady state solution in the computational domain. The equation for the angular momentum conservation (52) is reduced to

$$\dot{M}\sqrt{GM} = \Phi_k(r). \tag{68}$$

The new mass flux $(\rho v_z)_{n,k+1}$ is defined by the equation

$$j_{n,k+1} = \frac{\dot{M}_n \sqrt{GM}}{(\delta \Phi_k + (1-\delta)\dot{M}_n \sqrt{GM})} j_{n,k}, \tag{69}$$

where $\delta$ is the parameter of relaxation. This step means that, if the $\Phi(r)_k < \dot{M}_n(r)\sqrt{GM}$, then the mass flux from the point of the disk with radius $r$ increases and decreases if the opposite inequality takes place. Finally, we find the distribution of the mass flux $j_n$ which satisfies Equation (52). However, it still does not satisfy the conservation of the mass in the disk—Equation (30).
5. In this step, Equation (30) is solved taking the obtained mass distribution $j_n$ and boundary condition $\dot{M} = \dot{M}_{edge}$ at $r_{in}$. We obtain a new distribution of the accretion rate $\dot{M}_{n+1}$. This is the external iteration. After that, the entire procedure is repeated.

As a result of this entire procedure, the steady state solution of the problem of the wind outflow with boundary conditions, which satisfies Equations (52) and (30), is obtained. As an example of the procedure, we present the results of three consequent external iterations (iterations on $n$). Figure 5 shows the distribution of $\dot{M}_n$ and $\Phi_{(n,k)}$ at some $n$ and $k$. This is still not a fully converged solution. Nevertheless, there is a good coincidence of two curves at $r < 200$. At $r > 200$, the solution still has not converged. Here, we demonstrate the largest problem of the proposed method. While the convergence on the external iterations is rather fast, the internal iterations converge slowly. This happens for the following reason. The reaction of the wind on the variation of the mass flux of the wind at the base of the flow is delayed and this delay increases with $r$.

The toroidal magnetic field at the surface of the disk is defined by all the flow until the Alfvenic surface. According to the theory of steady state magnetized winds, the toroidal magnetic field is defined by regularity conditions at the Alfvenic surface [83,85]. Therefore, after variation of the mass flux at the base of the flow, the information about this event should propagate to the Alfvenic surface and return back to specify a new value of the toroidal magnetic field at the base. This delay can be estimated as the time $\tau$ necessary for a signal to travel from the surface of the disk to the Alfvenic surface. The signal propagates with the Alfvenic velocity $V_A = \frac{B}{\sqrt{4\pi\rho}}$. Travel time is estimated as $\tau \sim R_A/V_A$, where $R_A$ is proportional to $r$. Assuming that $V_A$ scales as $r^{-1/2}$ like the Keplerian velocity, $\tau$ scales as $r^{3/2}$. Then, in our case, the relaxation time of the flow at the outer edge of the disk exceeds the relaxation time at the inner edge by a factor of 1000. This explains the extremely slow convergence of the flow to the self-consistent solution.

Nevertheless, already obtained results convince us that the self-consistent solution of the cold accretion exists not only under the self similar assumptions. Apparently, at the magnetic field exceeding $B_{min}$, it is possible to find a density of the mass flow from the disk that will satisfy Equations (52) and (30) expressing mass and angular momentum conservation. This means that actually the solution of the problem depends only on distribution of the normal component of $B_z$ over the surface of the disk and accretion rate at the inner radius $\dot{M}_{edge}$. The mass flux distribution is defined at the solution of the self-consistent problem.

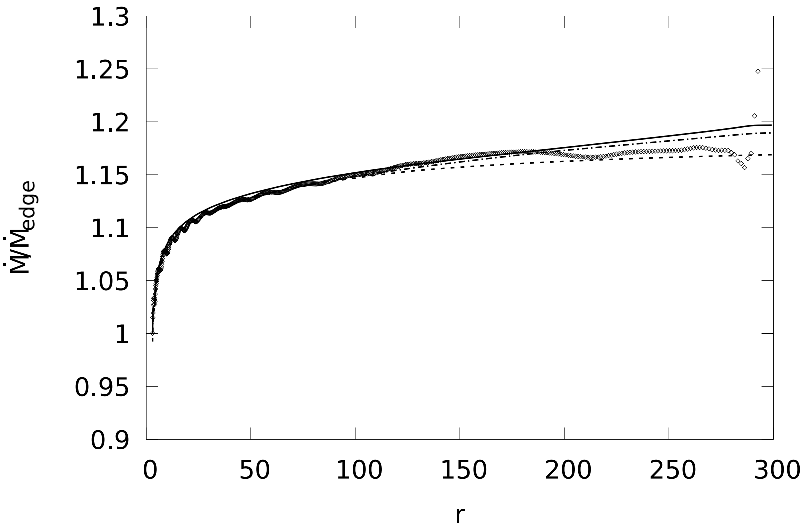


**Figure 5.** Distributions of $\dot{M}_{n+1}$ (solid line) and $\dot{M}_n$ (dashed-dotted line) and $\dot{M}_{n-1}$ in comparison with $\Phi_{n+1}$ (open circles) at some $n$.

## 8. Ratio of Kinetic to Bolometric Luminosity of the Disk

One of the main objectives of the model of the cold accretion is the explanation of the high ratio of the kinetic luminosity of jets from AGN over the bolometric luminosity of the disks. Therefore, one of the most important tests for the model is its ability to account for this ratio. In this section, we present an estimation of this ratio. Energy dissipated in the disk is defined by Equation (31). This energy is distributed among nonthermal and thermal radiation emitted by the disk. All together gives the bolometric luminosity of the disk. The rate of dissipation (31) depends on the thickness of the disk. Its calculation is possible only in a specific model of the disk structure. Here, we explore the SS model of geometrically thin but optically thick disk [3]. In this model,

$$t_{r\varphi} = -\alpha\rho v_s^2, \tag{70}$$

where $\alpha$ is the viscosity parameter, and the height of the disk above equatorial plane $h$ equals

$$h = r\frac{v_s}{V_k}. \tag{71}$$

Assumption (70) allows us to estimate the radial velocity of matter in the disk as follows

$$v_r = \frac{\alpha}{\theta}v_s\,. \tag{72}$$

This velocity essentially exceeds the radial velocity of matter in the SS disk at $\theta \sim 1$ because of the higher efficiency of the angular momentum loss. In accordance with the SS model, we assume that all the dissipated energy goes into heating of the disk and finally is carried out by thermal radiation from the disk surface.

### 8.1. Thermal Radiation from the Disk during "Cold" Accretion

In [3], three regimes of disk accretion were considered: (a) the radiation pressure exceeding the gas pressure and the Thomson scattering dominating over free–free absorption; (b) the gas pressure dominating over radiation pressure but the Thomson scattering dominating free–free absorption; and (c) the gas pressure dominating over radiation pressure and the opacity of the matter defined by free–free absorption. We consider only the cases when gas pressure dominates over radiation pressure. These are regimes (b) and (c). Below, we will see that, when radiation dominates, accretion proceeds in the Shakura–Sunayev regime.

### 8.2. Scattering Dominating over Free–Free Absorption

Firstly, we consider the case when Thomson scattering dominates over free–free absorption (Thomson regime). Radiation pressure $P_{rad}$ equals $\varepsilon/3$, where $\varepsilon = bT^4$. The sound velocity is defined as $v_s^2 = kT/m_p$, where $m_p$ is the proton mass. According to [3], the heat conductivity of the disk is defined by the transport of radiation. Then,

$$\varepsilon = \frac{3}{4}\frac{Q\sigma u_0}{c}, \tag{73}$$

where $\sigma = 0.4\ \ \mathrm{cm}^2/\mathrm{g}$ is the Thomson opacity, and $u_0 = 2\rho h$. The rate of heating of the disk follows from Equations (31), (51), (52) and equals

$$Q = \frac{3\theta \dot{M} V_k v_s}{16\pi r^2}. \tag{74}$$

We used here that $h = v_s/\Omega$. The solution of these two equations under assumption (70) yields the temperature inside the disk

$$T = \frac{\sqrt{3}}{4\sqrt{\pi}}\left(\frac{\theta^2 \dot{M}^2 V_k \sigma}{b\alpha c r^3}\right)^{\frac{1}{4}}. \tag{75}$$

The sound velocity equals

$$v_s = \frac{3^{1/4}}{2(\pi)^{1/4}}\frac{k^{1/2} V_k^{1/8} (\theta\dot{M})^{1/4} \sigma^{1/8}}{m_p^{1/2} b^{1/8} \alpha^{1/8} c^{1/8} r^{3/8}}, \tag{76}$$

and the density flux of radiation from one side of the disk is expressed as

$$Q = \frac{3^{5/4}}{32\pi^{5/4}}\frac{(\theta\dot{M})^{5/4} V_k^{9/8} k^{1/2} \sigma^{1/8}}{r^{19/8} m_p^{1/2} b^{1/8} \alpha^{1/8} c^{1/8}}. \tag{77}$$

Let us express $\dot{M} = \dot{m}\dot{M}_{Edd}$ , the radius $r$ in $r = (3r_g)x$ and the mass $M$ in the solar masses $M = mM_\odot$. In these variables, we obtain

$$Q = 0.77 \times 10^{23}\frac{(\theta\dot{m})^{5/4}}{m^{9/8} x^{47/16} \alpha^{1/8}},\ \ \mathrm{erg/s/cm^2}. \tag{78}$$

The integration of this expression over the disk gives the bolometric luminosity of the disk

$$L_{bol} = 0.84 \times 10^{36}\frac{(\theta\dot{m})^{5/4} m^{7/8}}{\alpha^{1/8}},\ \mathrm{erg/s}. \tag{79}$$

The ratio of $L_{bol}/L_{Edd}$ is

$$\frac{L_{bol}}{L_{Edd}} = 6 \times 10^{-3}\frac{(\theta\dot{m})^{5/4}}{(\alpha m)^{1/8}}. \tag{80}$$

The kinetic luminosity of the jets equals the total energy release of accretion. Therefore,

$$L_{kin} = \frac{\dot{M}c^2}{12} = 1.4 \times 10^{38} m\dot{m}, \text{ erg/s}. \tag{81}$$

Then, the ratio of the kinetic luminosity over the bolometric luminosity equals

$$\frac{L_{kin}}{L_{bol}} = 170 \frac{(m\alpha)^{1/8}}{\dot{m}^{1/4}\theta^{5/4}}. \tag{82}$$

The bolometric luminosity can be expressed in the conventional variables:

$$L_{bol} = \frac{4}{5}\theta \dot{M} V_{k0} v_{s0}, \tag{83}$$

where $V_{k0}$ and $v_{s0}$ are the Keplerian and sound velocities at the inner edge of the disk. Taking into account that the kinetic luminosity

$$L_{kin} = \frac{\dot{M}V_{k0}^2}{2}, \tag{84}$$

the condition $L_{bol}/L_{kin} \ll 1$ becomes

$$\frac{8}{5}\frac{\theta v_{s0}}{V_{k0}} = \frac{8}{5}\frac{\theta h}{r} \ll 1, \tag{85}$$

which practically coincides with the condition of applicability of the "cold" disk accretion approximation defined by Equation (50). A similar condition has been obtained earlier in [55]. The condition $L_{kin} \gg L_{bol}$ indicates that accretion occurs in the "cold" regime.

The temperature in the disk

$$T = 2.5 \times 10^7 \frac{\sqrt{\theta \dot{m}}}{\alpha^{1/4} x^{7/8} m^{1/4}}, \text{ K} \tag{86}$$

is less than the temperature in the Shakura–Sunyaev disk [3] disk results in $\theta \sim 1$.

Let us calculate the ratio of radiation pressure over the gas pressure in the disk,

$$\frac{P_{rad}}{P_{gas}} = \frac{3}{32\pi}\frac{\theta \dot{M}\sigma}{rc} = 0.85 \frac{\theta \dot{m}}{x}. \tag{87}$$

This means that all our estimates are valid when $0.85\theta\dot{m} < 1$. Other disk parameters are estimated as follows. The density equals

$$\rho = \frac{1}{2\sqrt{3\pi}} \frac{\sqrt{\theta \dot{M}} V_k^{3/4} m_p b^{1/4} c^{1/4}}{r^{5/4} k \alpha^{3/4} \sigma^{1/4}} = 0.6 \frac{\sqrt{\theta \dot{m}}}{m^{3/4} x^{13/8} \alpha^{3/4}}, \text{ g/cm}^3. \tag{88}$$

The aspect ratio of the disk is

$$\frac{h}{r} = 3.7 \times 10^{-3} \frac{(\dot{m}\theta)^{1/4} x^{1/16}}{(\alpha m)^{1/8}}. \tag{89}$$

The true optical depth $\tau^* = \sqrt{\sigma \cdot \sigma_{ff}} \cdot u_0$ of the disk is expressed as

$$\tau^* = 51(\theta \dot{m})^{1/8} m^{3/16} x^{5/32} \alpha^{-13/16}, \tag{90}$$

where $\sigma_{ff} = 0.11 \cdot T^{-7/2} n$, $\mathrm{cm}^2/\mathrm{g}$ is the free–free opacity of the disk. The surface temperature of the disk $T_S$ is defined from the equation $bcT_s^4/4 = Q$ and has the form

$$T_s = 5 \times 10^6 \frac{(\theta \dot{m})^{5/16}}{m^{9/32} x^{47/64} \alpha^{1/32}} \ \mathrm{K}. \tag{91}$$

### 8.3. Free–Free Absorption Dominating over Scattering

Under the condition

$$4.6 \times 10^{-3} \frac{(\alpha m)^{1/10} x^{23/20}}{(\theta \dot{m})} > 1\,, \tag{92}$$

free–free absorption exceeds Thomson scattering. Hereafter, we call this regime "free-free". Similar calculations yield the following temperature distribution inside the disk

$$T = 10^7 \frac{(\theta \dot{m})^{6/17}}{x^{12/17} (\alpha \cdot m)^{4/17}} \ \mathrm{K}. \tag{93}$$

The bolometric luminosity of the disk is

$$L_{bol} = 0.6 \times 10^{36} (\theta \dot{m})^{20/17} m^{15/17} \alpha^{-2/17} \ \mathrm{erg/s}, \tag{94}$$

while

$$\frac{L_{bol}}{L_{Edd}} = 4.4 \times 10^{-3} \frac{(\theta \dot{m})^{20/17}}{(\alpha m)^{2/17}}. \tag{95}$$

The ratio of kinetic luminosity over the bolometric luminosity equals

$$\frac{L_{kin}}{L_{bol}} = \frac{228 (\alpha m)^{2/17}}{\dot{m}^{3/17} \theta^{20/17}}. \tag{96}$$

The full optical depth, the density of plasma and the aspect ratio of the disk are given by

$$\tau = 93 (\theta \dot{m})^{4/17} m^{3/17} x^{1/34} \alpha^{-14/17}, \tag{97}$$

$$\rho = \frac{1.2 (\theta \dot{m})^{11/17}}{(\alpha m)^{13/17} \cdot x^{61/34}} \ \mathrm{g/cm^3}, \tag{98}$$

$$\frac{h}{r} = 2.5 \times 10^{-3} x^{5/34} (\theta \dot{m})^{3/17} (\alpha m)^{-2/17}, \tag{99}$$

respectively. The dissipated flux of energy per unit square from one side of the disk is

$$Q = 5.2 \times 10^{22} \frac{\theta^{20/17} \dot{m}^{20/17}}{m^{19/17} x^{97/34} \alpha^{2/17}}. \tag{100}$$

Finally, the surface temperature is equal to

$$T_s = 5.5 \times 10^6 \frac{(\theta \dot{m})^{5/17}}{m^{19/68} x^{97/136} \alpha^{1/34}} \ \mathrm{K}. \tag{101}$$

## 9. Comparison with the Fundamental Plane of Black Holes

The fundamental plane encapsulates the relationship between the compact radio luminosity, X-ray luminosity, and the black hole mass, and provides a good description of the data over a very large range of black hole masses. There are reasons to believe that the Fundamental Plane (hereafter, FP) of black holes reproduces the actual relationship between the kinetic luminosity of jets and the bolometric luminosity of the disks. In [29], the position of objects of different masses in the coordinates $L_{kin}/L_{bol}$ and $L_{bol}/L_{Edd}$ has been collected in one FP. If this is true, the FP can be used to extract information about the dependence of $\theta$ on $\dot{m}$ and $m$. All data at the FP can be approximated by a power law function of the form

$$\log \frac{L_{kin}}{L_{bol}} = (A-1)\log(\frac{L_{bol}}{L_{Edd}}) + B \quad (102)$$

with $A$ in the range (0.43–0.47) and $B$ in the range from $-0.94$ to $-1.37$. For our estimates, the values $A = 0.457$ and $B = -1.1$ around the average have been chosen.

If the empirical relationship (102) is valid, then

$$\frac{L_{bol}}{L_{Edd}} = 10^{-\frac{B}{A}} \dot{m}^{\frac{1}{A}}. \quad (103)$$

We used here that $L_{kin}/L_{Edd} = \dot{m}$ in the regime of "cold" accretion. This semi empirical relationship is very useful because it connects the bolometric luminosity of the disk with the accretion rate directly. The equations defining $L_{bol}$ and $L_{kin}/L_{bol}$ obtained for $A = 0.457$ and $B = -1.1$ are as follows:

$$L_{bol} = 3.6 \times 10^{40} m\dot{m}^{2.19} \text{ erg/s}\,, \quad (104)$$

and

$$\frac{L_{kin}}{L_{bol}} = 3.9 \times 10^{-3} \dot{m}^{-1.19}. \quad (105)$$

The empirical relationship (102) allows us to estimate $\theta$. Obviously, a constant $\theta$ is not consistent with observations. It must depend on $\dot{m}$ and $m$. It is natural to assume that $\theta$ depends on $\dot{m}$ as a power law

$$\theta = D\dot{m}^{\gamma}. \quad (106)$$

In the Thomson regime,

$$X = \frac{L_{bol}}{L_{Edd}} = 6 \times 10^{-3} \frac{\dot{m}^{5(\gamma+1)/4} D^{5/4}}{(\alpha m)^{1/8}}, \quad (107)$$

and

$$Y = \frac{L_{kin}}{L_{bol}} = \frac{168(\alpha m)^{1/8}}{D^{5/4}\dot{m}^{(5\gamma+1)/4}}. \quad (108)$$

After simple algebraic calculations, we obtain that $Y$ depends on $X$ as in Equation (102) if

$$A = \frac{4}{5(\gamma+1)}, \quad (109)$$

For $A = 0.457$, the value $\gamma = 3/4 = 0.75$. Then, the value $B = -1.1$ is obtained for $D = 5 \times 10^3 (\alpha m)^{1/10}$. Thus, in the Thomson regime,

$$\theta = 5 \times 10^3 \dot{m}^{3/4} (\alpha m)^{1/10}. \quad (110)$$

Similar calculations in the free–free regime yield

$$\theta = 11.2 \times 10^3 \dot{m}^{0.86} (\alpha m)^{1/10}. \quad (111)$$

The power of $\dot{m}$ is chosen so as to provide uniform dependence of $Y$ on $X$ of the form (102) with constant $A$ in both regimes.

The dependencies (110) and (111) look physically reasonable. They show that, the smaller the accretion rate, the more uniform is the magnetic field across the disk.

A plot of $\theta/(\alpha m)^{1/10}$ is presented in Figure 6. $\theta$ corresponding to FP agrees with the assumption of "cold" accretion because this curve is located well below the curve separating the regime of cold accretion from the Shakura–Sunyaev regime. In Figure 6, the dashed-dotted line separates regions of domination of the gas pressure and regions of domination of the radiation pressure as defined by Equation (87). The thin solid line separates the Thomson regime from the free–free regime.

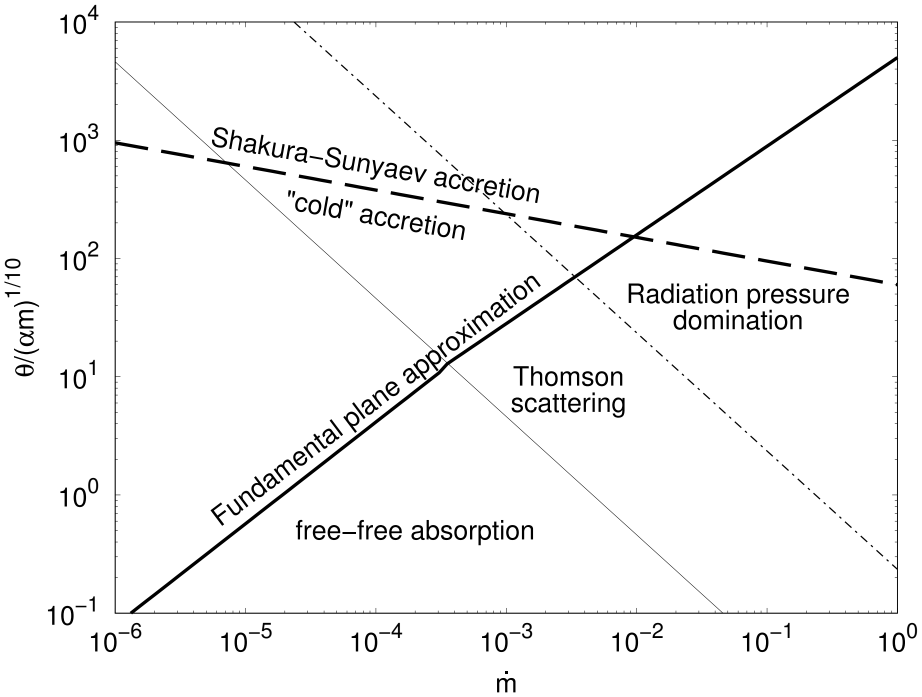


**Figure 6.** Dependence of $\theta/(\alpha m)^{1/10}$ on $\dot{m}$. The Shakura–Sunyaev accretion regime takes place above the thick dashed line. Below this line, the regime of "cold" accretion takes place. Thomson scattering dominates above the thin solid line, while, below this line, free–free absorption gives the major contribution in the opacity of the medium. The dashed-dotted line (calculated for $m = 10^8$) divides the plane in two parts where radiation pressure (above) and gas pressure (below) dominate.

## 10. Comparison with Specific Sources

It is interesting to apply the estimated dependencies to specific sources. Below, we consider M87 and the SMBH in the galactic center, Sgr A*. We will see below that both sources are in the free–free regime. Therefore, we used Equation (111) in our estimations. For ease of calculation, we consider the case with $\alpha = 0.1$.

### *10.1. M 87*

For this object, $\dot{m}$ and $m$ can be easily estimated. The kinetic luminosity of this object is $L_{kin} = 10^{44}$ erg/s, which we assume is equal to the total rate of gravitational energy released in the accretion. The mass of the central black hole is equal to $m = 3.5 \times 0^9$ [89]. With the Eddington luminosity equal to $L_{Edd} = 1.4 \times 10^{38} m$ erg/s, we find $\dot{m} = L_{kin}/L_{Edd} = 2 \times 10^{-4}$. From Equations (111) and (96), we obtain that $\theta = 54$ and $L_{kin}/L_{bol} \approx 95$. According to Equation (104), $L_{bol} = 10^{42}$ erg/s in accordance with observations. The optical depth of the disk exceeds $\tau > 10^4$.

### *10.2. Sgr A**

The mass of SMBH in Sgr A* is equal to $m = 4 \times 10^6$ while the bolometric luminosity is $L_{bol} \sim 10^{36}$ erg/s [34]. The kinetic luminosity of the outflow from the disk around SMBH in Sgr A* is not known. The flux of TeV gamma-rays from the Galactic Center can be explained by very high energy accelerated protons with a luminosity close to $10^{38}$ erg/s. The kinetic luminosity of the wind has to be higher. Let us estimate $\dot{m}$ from the bolometric luminosity of the disk (see Equation (104)). In this case, $\dot{m} = 8 \times 10^{-6}$ and $\theta = 1.7$ at $\tau \sim 10^3$. The value of $\dot{m}$ agrees with estimates of the accretion rate obtained from Bondi accretion of stellar winds of the order of $10^{21}$ g/s [90]. From Equation (81), we obtain that

$$L_{kin} = 4.4 \times 10^{39} \text{ erg/s} . \tag{112}$$

The kinetic luminosity of the wind from the Galactic accretion disk exceeds the bolometric luminosity of the disk $4.4 \times 10^3$ times. Remarkably, this power is sufficient to explain the flux of PeV protons from the Galactic Center.

## 11. Conclusions

The main energy release in the AGNs occurs as a flux of kinetic energy of the jets. The question of the energy source of the jets is the main question to which the theory must first answer. There are two answers to this question. In the first case, the main source of energy of the jet is the energy of rotation of the black hole which is transformed into energy of $e^{\pm}$ jets due to the Blandford and Znajek mechanism [42]. Only a small fraction of the gravitational energy of the accreted matter is released in the form of radiation of the disk. The major part of the gravitational energy goes into increasing the mass of the SMBH. This model needs additional assumptions. Accretion has to occur in the ADAF regime to provide radiatively inefficient disks. The speed of rotation of the SMBH must be close to the maximal possible and accretion must occur in the regime of the Magnetically Arrested Disks. In this regime, the magnetic field is so strong that it destroys the disk. Otherwise, it is not possible to provide the necessary energetics of jets.

In another case of "cold" accretion, the only source of energy is the gravitational energy of the accreted matter. The major part of this energy goes into the energy of magnetized wind and a small fraction of the energy is released in the form of radiation from the disk. An attractive feature of this model is a natural explanation for the high kinetic power of the jets compared to the luminosity of the accretion disk. As a bonus, the kinetic energy of particles in a jet can be orders of magnitude greater than the kinetic energy of particles in a Kepler orbit.

"Cold" accretion does not need special conditions or exotic magnetic fields. This regime of accretion is implemented when a magnetized wind expires from the disk. The existence of the winds from the disks is confirmed by numerous observations. "Cold" accretion goes into Shakura–Sunyaev accretion [3] when the loss of the angular momentum due to viscose stresses dominates the loss due to the wind. Nevertheless, "cold" accretion occurs even when the magnetic field inside the accretion disk essentially exceeds the magnetic field at the base of the wind. This is explained by geometry. The angular momentum transport due to viscosity is proportional to the magnetic pressure in the disk times the thickness of the disk $h$ while the flux of the angular momentum from the disk is proportional to the magnetic pressure at the base of the wind times the radius $r$. The ratio of viscous losses to losses due to the wind is $\sim\theta \cdot (\frac{h}{r})$, where $\theta$ roughly equals the ratio of magnetic pressures inside and at the surface of the disk. Therefore, the Shakura–Sunyaev regime of accretion is realized when $\theta > (\frac{r}{h})$.

Estimates of the ratio of the kinetic luminosity of the jets to the bolometric luminosity of the disk show that the current observations can be explained in the framework of "cold" accretion. Of course, the assumption that $\theta$ is constant evidently contradicts observations. Detailed comparison of the theoretical predictions with the Fundamental plane of the black holes shows that $\theta$ has to increase two orders of magnitude with $\dot{m}$. This behavior of $\theta$ agrees with the results of modeling of the magnetic field distribution in the disk [72]. This estimate allows us to obtain certain conclusions about the realization of the regime of "cold" disk accretion. At small accretion rates $\dot{m} < 10^{-2}$, the estimated value of $\theta$ lies in the region well below the line where the Shakura–Sunyaev model is valid. The magnetic pressure inside the disk appears less than the magnetic pressure estimated in the model [3]. It is reasonable to assume that, at relatively low rates of accretion, $\dot{m} < 10^{-2}$, accretion occurs predominantly in the regime of "cold" accretion. At higher values of $\dot{m} > 0.1$, the accretion occurs in the regime of Shakura and Sunyaev. The transition between the two regimes takes place at a value of $\dot{m}$ between 0.01 and 0.1 that agrees well with the transition from very bright to very dim disks around SMBH with powerful outflows deduced in [41]. Remarkably, the rough estimate of the dependence of $\theta$ on $\dot{m}$ gives good agreements with observations of two SMBHs, M87 and Sgr A*. It is highly unlikely that such an agreement could be accidental.

**Funding:** This research was funded by the Russian Science Foundation project N 16-12-10443.

**Conflicts of Interest:** The authors declare no conflict of interest.

## References

1. Shakura, N.I. Disk Model of Gas Accretion on a Relativistic Star in a Close Binary System. *Sov. Astron.* **1972**, *49*, 921.
2. Pringle, J.E.; Rees, M.J. Accretion Disc Models for Compact X-Ray Sources. *Astron. Astrophys.* **1972**, *21*, 1.
3. Shakura, N.I.; Sunyaev, R.A. Black holes in binary systems. Observational appearance. *Astron. Astrophys.* **1973**, *24*, 337–355.
4. Baganoff, F.K.; Maeda, Y.; Morris, M.; Bautz, M.W.; Brandt, W.N.; Cui, W.; Doty, J.P.; Feigelson, E.D.; Garmire, G.P.; Pravdo, S.H.; et al. Chandra X-Ray Spectroscopic Imaging of Sagittarius A* and the Central Parsec of the Galaxy. *Astrophys. J.* **2003**, *591*, 891–915. [CrossRef]
5. Narayan, R.; Yi, I. Advection-dominated Accretion: Underfed Black Holes and Neutron Stars. *Astrophys. J.* **1995**, *452*, 710. [CrossRef]
6. Bisnovatyi-Kogan, G.S.; Lovelace, R.V.E. Influence of Ohmic Heating on Advection-dominated Accretion Flows. *Astrophys. J.* **1997**, *486*, 43–46. [CrossRef]
7. Quataert, E.; Gruzinov, A. Convection-dominated Accretion Flows. *Astrophys. J.* **2000**, *539*, 809–814. [CrossRef]
8. Narayan, R.; Quataert, E.; Igumenshchev, I.V.; Abramowicz, M.A. The Magnetohydrodynamics of Convection-dominated Accretion Flows. *Astrophys. J.* **2002**, *577*, 295–301. [CrossRef]
9. Blandford, R.D.; Begelman, M.C. On the fate of gas accreting at a low rate on to a black hole. *Mon. Not. R. Astron. Soc.* **1999**, *303*, 1–5. [CrossRef]
10. Stone, J.M.; Pringle, J.E.; Begelman, M.C. Hydrodynamical non-radiative accretion flows in two dimensions. *Mon. Not. R. Astron. Soc.* **1999**, *310*, 1002–1016. [CrossRef]
11. Blandford, R.D.; Begelman, M.C. Two-dimensional adiabatic flows on to a black hole—I. Fluid accretion. *Mon. Not. R. Astron. Soc.* **2004**, *349*, 68–86. [CrossRef]
12. Falcke, H.; Markoff, S. The jet model for Sgr A*: Radio and X-ray spectrum. *Astron. Astrophys.* **2000**, *362*, 113–118.
13. Yuan, F.; Markoff, S.; Falcke, H. A Jet-ADAF model for Sgr A$^*$. *Astron. Astrophys.* **2002**, *383*, 854–863. [CrossRef]
14. Bicknell, G.V.; Begelman, M.C. Understanding the Kiloparsec-Scale Structure of M87. *Astrophys. J.* **1996**, *467*, 597. [CrossRef]
15. Reynolds, C.S.; Di Matteo, T.; Fabian, A.C.; Hwang, U.; Canizares, C.R. The 'quiescent' black hole in M87. *Mon. Not. R. Astron. Soc.* **1996**, *283*, 111–116. [CrossRef]
16. Biretta, J.A.; Stern, C.P.; Harris, D.E. The radio to X-ray spectrum of the M87 jet and nucleus. *Astron. J.* **1991**, *101*, 1632–1646. [CrossRef]
17. Rawlings, S.; Saunders, R. Evidence for a common central-engine mechanism in all extragalactic radio sources. *Nature* **1991**, *349*, 138–140. [CrossRef]
18. Heinz, S.; Sunyaev, R.A. The non-linear dependence of flux on black hole mass and accretion rate in core-dominated jets. *Mon. Not. R. Astron. Soc.* **2003**, *343*, 59–64. [CrossRef]
19. Merloni, A.; Heinz, S.; di Matteo, T. A Fundamental Plane of black hole activity. *Mon. Not. R. Astron. Soc.* **2003**, *345*, 1057–1076. [CrossRef]
20. Falcke, H.; Körding, E.; Markoff, S. A scheme to unify low-power accreting black holes. Jet-dominated accretion flows and the radio/X-ray correlation. *Astron. Astrophys.* **2004**, *414*, 895–903. [CrossRef]
21. Körding, E.G.; Fender, R.P.; Migliari, S. Jet-dominated advective systems: Radio and X-ray luminosity dependence on the accretion rate. *Mon. Not. R. Astron. Soc.* **2006**, *369*, 1451–1458. [CrossRef]
22. Merloni, A.; Heinz, S. Measuring the kinetic power of active galactic nuclei in the radio mode. *Mon. Not. R. Astron. Soc.* **2007**, *381*, 589–601. [CrossRef]

23. De Gasperin, F.; Merloni, A.; Sell, P.; Best, P.; Heinz, S.; Kauffmann, G. Testing black hole jet scaling relations in low-luminosity active galactic nuclei. *Mon. Not. R. Astron. Soc.* **2011**, *415*, 2910–2919. [CrossRef]
24. Saikia, P.; Körding, E.; Falcke, H. The Fundamental Plane of black hole activity in the optical band. *Mon. Not. R. Astron. Soc.* **2015**, *450*, 2317–2326. [CrossRef]
25. Körding, E.G.; Jester, S.; Fender, R. Measuring the accretion rate and kinetic luminosity functions of supermassive black holes. *Mon. Not. R. Astron. Soc.* **2008**, *383*, 277–288. [CrossRef]
26. Ma, M.L.; Cao, X.W.; Jiang, D.R.; Gu, M.F. A New Approach for Estimating Kinetic Luminosity of Jet in AGNs. *Chin. J. Astron. Astrophys.* **2008**, *8*, 39–49. [CrossRef]
27. López-Corredoira, M.; Perucho, M. Kinetic power of quasars and statistical excess of MOJAVE superluminal motions. *Astron. Astrophys.* **2012**, *544*, A56. [CrossRef]
28. Daly, R.A. Spin properties of supermassive black holes with powerful outflows. *Mon. Not. R. Astron. Soc.* **2016**, *458*, 24–28. [CrossRef]
29. Daly, R.A.; Stout, D.A.; Mysliwiec, J.N. The Fundamental Plane of Black Hole Activity Represented in Terms of Dimensionless Beam Power and Bolometric Luminosity. *arXiv* **2016**, arXiv:1606.01399.
30. Fernandes, C.A.C.; Jarvis, M.J.; Rawlings, S.; Martínez-Sansigre, A.; Hatziminaoglou, E.; Lacy, M.; Page, M.J.; Stevens, J.A.; Vardoulaki, E. Evidence for a maximum jet efficiency for the most powerful radio galaxies. *Mon. Not. R. Astron. Soc.* **2011**, *411*, 1909–1916. [CrossRef]
31. Punsly, B. High Jet Efficiency and Simulations of Black Hole Magnetospheres. *Astrophys. J.* **2011**, *728*, 17. [CrossRef]
32. Ghisellini, G.; Tavecchio, F.; Maraschi, L.; Celotti, A.; Sbarrato, T. The power of relativistic jets is larger than the luminosity of their accretion disks. *Nature* **2014**, *515*, 376–378. [CrossRef]
33. Abramowski, A.; Aharonian, F.; Benkhali, F.A.; Akhperjanian, A.G.; Angüner, E.O.; Backes, M.; Balzer, A.; Becherini, Y.; Tjus, J.B.; Berge, D.; et al. Acceleration of petaelectronvolt protons in the Galactic Centre. *Nature* **2016**, *531*, 476–479. [CrossRef]
34. Genzel, R.; Eisenhauer, F.; Gillessen, S. The Galactic Center massive black hole and nuclear star cluster. *Rev. Mod. Phys.* **2010**, *82*, 3121–3195. [CrossRef]
35. Striani, E.; Vercellone, S.; Tavani, M.; Vittorini, V.; D'Ammando, F.; Donnarumma, I.; Pacciani, L.; Pucella, G.; Bulgarelli, A.; Trifoglio, M.; et al. The Extraordinary Gamma-ray Flare of the Blazar 3C 454.3. *Astrophys. J.* **2010**, *718*, 455–459. [CrossRef]
36. Ackermann, M.; Ajello, M.; Baldini, L.; Ballet, J.; Barbiellini, G.; Bastieri, D.; Bechtol, K.; Bellazzini, R.; Berenji, B.; Blandford, R.D.; et al. Fermi Gamma-ray Space Telescope Observations of Gamma-ray Outbursts from 3C 454.3 in 2009 December and 2010 April. *Astrophys. J.* **2010**, *721*, 1383–1396. [CrossRef]
37. Vercellone, S.; Striani, E.; Vittorini, V.; Donnarumma, I.; Pacciani, L.; Pucella, G.; Tavani, M.; Raiteri, C.M.; Villata, M.; Romano, P.; et al. The Brightest Gamma-Ray Flaring Blazar in the Sky: AGILE and Multi-wavelength Observations of 3C 454.3 During 2010 November. *Astrophys. J.* **2011**, *736*, L38. [CrossRef]
38. Abdo, A.A.; Ackermann, M.; Ajello, M.; Allafort, A.; Baldini, L.; Ballet, J.; Barbiellini, G.; Bastieri, D.; Bellazzini, R.; Berenji, B.; et al. Fermi Gamma-ray Space Telescope Observations of the Gamma-ray Outburst from 3C454.3 in November 2010. *Astrophys. J.* **2011**, *733*, 26. [CrossRef]
39. Khangulyan, D.V.; Barkov, M.V.; Bosch-Ramon, V.; Aharonian, F.A.; Dorodnitsyn, A.V. Star-Jet Interactions and Gamma-Ray Outbursts from 3C454.3. *Astrophys. J.* **2013**, *774*, 113. [CrossRef]
40. Pjanka, P.; Zdziarski, A.A.; Sikora, M. The power and production efficiency of blazar jets. *Mon. Not. R. Astron. Soc.* **2017**, *465*, 3506–3514. [CrossRef]
41. Churazov, E.; Sazonov, S.; Sunyaev, R.; Forman, W.; Jones, C.; Böhringer, H. Supermassive black holes in elliptical galaxies: Switching from very bright to very dim. *Mon. Not. R. Astron. Soc.* **2005**, *363*, L91–L95. [CrossRef]
42. Blandford, R.D.; Znajek, R.L. Electromagnetic extraction of energy from Kerr black holes. *Mon. Not. R. Astron. Soc.* **1977**, *179*, 433–456. [CrossRef]
43. Narayan, R.; Igumenshchev, I.V.; Abramowicz, M.A. Magnetically Arrested Disk: An Energetically Efficient Accretion Flow. *Publ. Astron. Soc. Jpn.* **2003**, *55*, L69–L72. [CrossRef]
44. Bisnovatyi-Kogan, G.S.; Ruzmaikin, A.A. The accretion of matter by a collapsing star in the presence of a magnetic field. II—self-consistent stationary picture. *Astrophys. Space Sci.* **1976**, *42*, 401–424. [CrossRef]

45. McKinney, J.C.; Tchekhovskoy, A.; Blandford, R.D. General relativistic magnetohydrodynamic simulations of magnetically choked accretion flows around black holes. *Mon. Not. R. Astron. Soc.* **2012**, *423*, 3083–3117. [CrossRef]
46. Parker, E.N. Dynamics of the Interplanetary Gas and Magnetic Fields. *Astrophys. J.* **1958**, *128*, 664. [CrossRef]
47. Schatzman, E. A theory of the role of magnetic activity during star formation. *Ann. d'Astrophys.* **1962**, *25*, 18.
48. Mestel, L. Magnetic braking by a stellar wind—I. *Mon. Not. R. Astron. Soc.* **1968**, *138*, 359. [CrossRef]
49. Mestel, L. Magnetic braking by a stellar wind—II. *Mon. Not. R. Astron. Soc.* **1968**, *140*, 177. [CrossRef]
50. Blandford, R.D.; Payne, D.G. Hydromagnetic flows from accretion discs and the production of radio jets. *Mon. Not. R. Astron. Soc.* **1982**, *199*, 883–903. [CrossRef]
51. Pelletier, G.; Pudritz, R.E. Hydromagnetic disk winds in young stellar objects and active galactic nuclei. *Astrophys. J.* **1992**, *394*, 117–138. [CrossRef]
52. Ferreira, J.; Pelletier, G. Magnetized accretion-ejection structures. 1. General statements. *Astron. Astrophys.* **1993**, *276*, 625.
53. Ferreira, J.; Pelletier, G. Magnetized accretion-ejection structures. III. Stellar and extragalactic jets as weakly dissipative disk outflows. *Astron. Astrophys.* **1995**, *295*, 807.
54. Ferreira, J. Magnetically-driven jets from Keplerian accretion discs. *Astron. Astrophys.* **1997**, *319*, 340–359.
55. Ferreira, J.; Petrucci, P.O.; Henri, G.; Saugé, L.; Pelletier, G. A unified accretion-ejection paradigm for black hole X-ray binaries. I. The dynamical constituents. *Astron. Astrophys.* **2006**, *447*, 813–825. [CrossRef]
56. Lubow, S.H.; Papaloizou, J.C.B.; Pringle, J.E. On the Stability of Magnetic Wind-Driven Accretion Discs. *Mon. Not. R. Astron. Soc.* **1994**, *268*, 1010. [CrossRef]
57. Livio, M.; Pringle, J.E.; King, A.R. The Disk-Jet Connection in Microquasars and Active Galactic Nuclei. *Astrophys. J.* **2003**, *593*, 184–188. [CrossRef]
58. Cao, X.; Spruit, H.C. The Large-scale Magnetic Fields of Thin Accretion Disks. *Astrophys. J.* **2013**, *765*, 149. [CrossRef]
59. Li, S.L.; Begelman, M.C. Thermal Stability of a Thin Disk with Magnetically Driven Winds. *Astrophys. J.* **2014**, *786*, 6. [CrossRef]
60. Li, S.L. The High-efficiency Jets Magnetically Accelerated from a Thin Disk in Powerful Lobe-dominated FRII Radio Galaxies. *Astrophys. J.* **2014**, *788*, 71. [CrossRef]
61. Marcel, G.; Ferreira, J.; Petrucci, P.; Henri, G.; Belmont, R.; Clavel, M.; Malzac, J.; Coriat, M.; Corbel, S.; Rodriguez, J.; et al. A unified accretion-ejection paradigm for black hole X-ray binaries. II. Observational signatures of jet-emitting disks. *arXiv* **2018**, arXiv:1803.04335.
62. Marcel, G.; Ferreira, J.; Petrucci, P.; Belmont, R.; Malzac, J.; Clavel, M.; Henri, G.; Coriat, M.; Corbel, S.; Rodriguez, J.; et al. A unified accretion-ejection paradigm for black hole X-ray binaries. III. Spectral signatures of hybrid disk configurations. *Astron. Astrophys.* **2018**, *617*, A46. [CrossRef]
63. Bogovalov, S.V.; Kelner, S.R. Accretion and Plasma Outflow from Dissipationless Discs. *Int. J. Mod. Phys. D* **2010**, *19*, 339–365. [CrossRef]
64. Bisnovatyi-Kogan, G.S.; Ruzmaikin, A.A. The Accretion of Matter by a Collapsing Star in the Presence of a Magnetic Field. *Astrophys. Space Sci.* **1974**, *28*, 45–59. [CrossRef]
65. Van Ballegooijen, A.A. Magnetic fields in the accretion disks of cataclysmic variables. In *Accretion Disks and Magnetic Fields in Astrophysics*; Belvedere, G., Ed.; Springer: Dordrecht, The Netherlands, 1989; pp. 99–106.
66. Lubow, S.H.; Papaloizou, J.C.B.; Pringle, J.E. Magnetic field dragging in accretion discs. *Mon. Not. R. Astron. Soc.* **1994**, *267*, 235–240. [CrossRef]
67. Bisnovatyi-Kogan, G.S.; Lovelace, R.V.E. Large-Scale B-Field in Stationary Accretion Disks. *Astrophys. J.* **2007**, *667*, L167–L169. [CrossRef]
68. Bisnovatyi-Kogan, G.S.; Lovelace, R.V.E. Vertical Structure of Stationary Accretion Disks with a Large-scale Magnetic Field. *Astrophys. J.* **2012**, *750*, 109. [CrossRef]
69. Galeev, A.A.; Rosner, R.; Vaiana, G.S. Structured coronae of accretion disks. *Astrophys. J.* **1979**, *229*, 318–326. [CrossRef]
70. Begelman, M.C.; Armitage, P.J. A Mechanism for Hysteresis in Black Hole Binary State Transitions. *Astrophys. J.* **2014**, *782*, L18. [CrossRef]
71. Begelman, M.C.; Armitage, P.J.; Reynolds, C.S. Accretion Disk Dynamo as the Trigger for X-Ray Binary State Transitions. *Astrophys. J.* **2015**, *809*, 118. [CrossRef]

72. Salvesen, G.; Simon, J.B.; Armitage, P.J.; Begelman, M.C. Accretion disc dynamo activity in local simulations spanning weak-to-strong net vertical magnetic flux regimes. *Mon. Not. R. Astron. Soc.* **2016**, *457*, 857–874. [CrossRef]
73. Riols, A.; Rincon, F.; Cossu, C.; Lesur, G.; Ogilvie, G.I.; Longaretti, P.Y. Magnetorotational dynamo chimeras. The missing link to turbulent accretion disk dynamo models? *Astron. Astrophys.* **2017**, *598*, A87. [CrossRef]
74. Contopoulos, I.; Kazanas, D. A Cosmic Battery. *Astrophys. J.* **1998**, *508*, 859–863. [CrossRef]
75. Contopoulos, I.; Nathanail, A.; Katsanikas, M. The Cosmic Battery in Astrophysical Accretion Disks. *Astrophys. J.* **2015**, *805*, 105. [CrossRef]
76. Bisnovatyi-Kogan, G.S.; Lovelace, R.V.E.; Belinski, V.A. A Cosmic Battery Reconsidered. *Astrophys. J.* **2002**, *580*, 380–388. [CrossRef]
77. Romanova, M.M.; Ustyugova, G.V.; Koldoba, A.V.; Chechetkin, V.M.; Lovelace, R.V.E. Dynamics of Magnetic Loops in the Coronae of Accretion Disks. *Astrophys. J.* **1998**, *500*, 703–713. [CrossRef]
78. Parfrey, K.; Giannios, D.; Beloborodov, A.M. Black hole jets without large-scale net magnetic flux. *Mon. Not. R. Astron. Soc.* **2015**, *446*, L61–L65. [CrossRef]
79. Crooker, N.U.; Burton, M.E.; Siscoe, G.L.; Kahler, S.W.; Gosling, J.T.; Smith, E.J. Solar wind streamer belt structure. *J. Geophys. Res.* **1996**, *101*, 24331–24342. [CrossRef]
80. Kahler, S.; Crooker, N.U.; Gosling, J.T. Properties of interplanetary magnetic sector boundaries based on electron heat-flux flow directions. *J. Geophys. Res.* **1998**, *103*, 20603–20612. [CrossRef]
81. Landau, L.D.; Lifshitz, E.M. *Electrodynamics of Continuous Media*; Elsevier: Amsterdam, The Netherlands, 1960.
82. Landau, L.D.; Lifshitz, E.M. *The Classical Theory of Fields*; Elsevier: Amsterdam, The Netherlands, 1975.
83. Bogovalov, S.V. Boundary conditions and critical surfaces in astrophysical MHD winds. *Astron. Astrophys.* **1997**, *323*, 634–643.
84. Contopoulos, J. General Axisymmetric Magnetohydrodynamic Flows: Theory and Solutions. *Astrophys. J.* **1996**, *460*, 185. [CrossRef]
85. Bogovalov, S.V. On the Theory of Magnetohydrodynamic Winds from a Magnetosphere of Axisymmetric Rotators. *Mon. Not. R. Astron. Soc.* **1994**, *270*, 721. [CrossRef]
86. Fukumura, K.; Kazanas, D.; Shrader, C.; Behar, E.; Tombesi, F.; Contopoulos, I. Magnetized Disk Winds in NGC 3783. *Astrophys. J.* **2018**, *853*, 40. [CrossRef]
87. Bogovalov, S.V.; Tronin, I.V. Numerical simulations of dissipationless disk accretion. *Astron. Lett.* **2017**, *43*, 595–601. [CrossRef]
88. Bogovalov, S.V.; Tronin, I.V. Toward the self-consistent model of cold disk accretion. *Int. J. Mod. Phys. D* **2018**, *27*, 1844005. [CrossRef]
89. Walsh, J.L.; Barth, A.J.; Ho, L.C.; Sarzi, M. The M87 Black Hole Mass from Gas-dynamical Models of Space Telescope Imaging Spectrograph Observations. *Astrophys. J.* **2013**, *770*, 86. [CrossRef]
90. Di Matteo, T.; Quataert, E.; Allen, S.W.; Narayan, R.; Fabian, A.C. Low-radiative-efficiency accretion in the nuclei of elliptical galaxies. *Mon. Not. R. Astron. Soc.* **2000**, *311*, 507–521. [CrossRef]